

# Numerical experiments of adjusted BSSN systems for controlling constraint violations

Kenta Kiuchi<sup>1</sup> \* and Hisa-aki Shinkai<sup>2</sup> †

<sup>1</sup>*Department of Physics, Waseda University, 3-4-1 Okubo, Shinjuku-ku, Tokyo 169-8555, Japan and*

<sup>2</sup>*Faculty of Information Science and Technology, Osaka Institute of Technology,  
1-79-1 Kitayama, Hirakata, Osaka 573-0196, Japan*

(Dated: December 24, 2018)

We present our numerical comparisons between the BSSN formulation widely used in numerical relativity today and its adjusted versions using constraints. We performed three testbeds: gauge-wave, linear wave, and Gowdy-wave tests, proposed by the Mexico workshop on the formulation problem of the Einstein equations. We tried three kinds of adjustments, which were previously proposed from the analysis of the constraint propagation equations, and investigated how they improve the accuracy and stability of evolutions. We observed that the signature of the proposed Lagrange multipliers are always right and the adjustments improve the convergence and stability of the simulations. When the original BSSN system already shows satisfactory good evolutions (e.g., linear wave test), the adjusted versions also coincide with those evolutions; while in some cases (e.g., gauge-wave or Gowdy-wave tests) the simulations using the adjusted systems last 10 times as long as those using the original BSSN equations. Our demonstrations imply a potential to construct a robust evolution system against constraint violations even in highly dynamical situations.

PACS numbers: 04.20.-q, 04.25.Dm, 04.25.-g

## I. INTRODUCTION

Numerical integration of the Einstein equations is the only way to investigate highly dynamical and nonlinear gravitational space-time. The detection of gravitational wave requires templates of waveform, among them mergers of compact objects are the most plausible astrophysical sources. Numerical relativity has been developed with this purpose over decades.

For neutron star (NS) binaries, a number of scientific numerical simulations have been done so far, and we are now at the level of discussing the actual physics of the phenomena, including the effects of the equations of state, hydrodynamics, and general relativity by evolving various initial data [1, 2, 3, 4, 5]. Mergers of black holes (BHs) are also available after the breakthrough by Pretorius [6] in 2004. Pretorius's implementation had many novel features in his code; among them he discretizes the four-dimensional Einstein equations directly, which is not a conventional approach so far. However, after the announcements of successful binary BH mergers by Campanelli et al. [7] and Baker et al. [8] based on the standard 3+1 decomposition of the Einstein equations, many groups began producing interesting results [9, 10, 11, 12, 13, 14, 15, 16, 17, 18]. The merger of NS-BH binary simulations has also been reported recently, e.g. [19].

Almost all the groups which apply the above conventional approach use the so-called BSSN variables together with “1 + log”-type slicing conditions for the lapse function and “ $\Gamma$ -driver” type slicing conditions for the shift

function. BSSN stands for Baumgarte-Shapiro [20] and Shibata-Nakamura [21], the modified Arnowitt-Deser-Misner formulation initially proposed by Nakamura [22]. (The details are described in §II A.) There have already been several efforts to explain why the combination of this recipe works from the point of view of the well-posedness of the partial differential equations (e.g. [23, 24]). However, the question remains whether there exists an alternative evolution system that enables more long-term stable and accurate simulations. The search for a better set of equations for numerical integrations is called the formulation problem for numerical relativity, of which earlier stages are reviewed by one of the authors [25].

In this article, we report our numerical tests of modified versions of the BSSN system, the *adjusted BSSN systems*, proposed by Yoneda and Shinkai [26]. The idea of their modifications is to add constraints to the evolution equations like Lagrange multipliers and to construct a robust evolution system which evolves to the constraint surface as the attractor. Their proposals are based on the eigenvalue analysis of the constraint propagation equations (the evolution equations of the constraints) on the perturbed metric. For the ADM formulation, they explain why the standard ADM does not work for long-term simulations by showing the existence of the constraint violating mode in perturbed Schwarzschild space-time [27]. For the BSSN formulation, they analyzed the eigenvalues of the constraint propagation equations only on flat space-time [26], but one of their proposed adjustments was immediately tested by Yo et al. [28] for the numerical evolution of Kerr-Schild space-time and confirmed to work as expected. (The details are described in §II B.)

Our numerical examples are taken from the proposed problems for testing the formulations of the Mexico Numerical Relativity Workshop 2001 participants [29],

---

\*kiuchi@gravity.phys.waseda.ac.jp

†shinkai@is.oit.ac.jp

which are sometimes called the Apples-with-Apples test. To concentrate the comparisons on the formulation problem, the templated problems are settled so as not to require technical complications; e.g., periodic boundary conditions are used and the slicing conditions do not require solving elliptical equations. Several groups already reported their code tests using these Apples tests (e.g. [30, 31, 32]), and we are also able to compare our results with theirs.

This article is organized as follows. We describe the BSSN equations and the *adjusted* BSSN equations in Sec. II A and II B. We give our three numerical test problems in Sec. III. Comments on our coding stuff are in Sec. IV. Sec. V is devoted to showing numerical results for each testbeds, and we summarize the results in Sec. VI.

## II. BASIC EQUATIONS

### A. BSSN equations

We start by presenting the standard BSSN formulation, where we follow the notations of [20], which are

widely used among numerical relativists.

The idea of the BSSN formulation is to introduce auxiliary variables to those of the Arnowitt-Deser-Misner (ADM) formulation for obtaining longer stable numerical simulations. The basic variables of the BSSN formulation are  $(\phi, \tilde{\gamma}_{ij}, K, \tilde{A}_{ij}, \tilde{\Gamma}^i)$ , which are defined by

$$\phi = \frac{1}{12} \log(\det \gamma_{ij}), \quad (2.1)$$

$$\tilde{\gamma}_{ij} = e^{-4\phi} \gamma_{ij}, \quad (2.2)$$

$$K = \gamma^{ij} K_{ij}, \quad (2.3)$$

$$\tilde{A}_{ij} = e^{-4\phi} \left[ K_{ij} - \frac{1}{3} \gamma_{ij} K \right], \quad (2.4)$$

$$\tilde{\Gamma}^i = \tilde{\gamma}^{jk} \tilde{\Gamma}_{jk}^i, \quad (2.5)$$

where  $(\gamma_{ij}, K_{ij})$  are the intrinsic and extrinsic ADM 3-metric. The conformal factor  $\phi$  is introduced so as to set  $\tilde{\gamma} \equiv \det[\tilde{\gamma}_{ij}]$  as unity,  $\tilde{A}_{ij}$  is supposed to be traceless, and  $\tilde{\Gamma}^i$  is treated independently in evolution equations. Therefore these three requirements turn into the new constraints [below (2.16)-(2.18)].

The set of the BSSN evolution equations are

$$\partial_t \phi = -\frac{1}{6} \alpha K + \beta^i \partial_i \phi + \frac{1}{6} \partial_i \beta^i, \quad (2.6)$$

$$\partial_t \tilde{\gamma}_{ij} = -2\alpha \tilde{A}_{ij} + \tilde{\gamma}_{ik} \partial_j \beta^k + \tilde{\gamma}_{jk} \partial_i \beta^k - \frac{2}{3} \tilde{\gamma}_{ij} \partial_k \beta^k + \beta^k \partial_k \tilde{\gamma}_{ij}, \quad (2.7)$$

$$\partial_t K = -D^i D_i \alpha + \alpha \tilde{A}_{ij} \tilde{A}^{ij} + \frac{1}{3} \alpha K^2 + \beta^i \partial_i K, \quad (2.8)$$

$$\begin{aligned} \partial_t \tilde{A}_{ij} = & -e^{-4\phi} [D_i D_j \alpha + \alpha R_{ij}]^{\text{TF}} + \alpha K \tilde{A}_{ij} - 2\alpha \tilde{A}_{ik} \tilde{A}^k_j \\ & + \partial_i \beta^k \tilde{A}_{kj} + \partial_j \beta^k \tilde{A}_{ki} - \frac{2}{3} \partial_k \beta^k \tilde{A}_{ij} + \beta^k \partial_k \tilde{A}_{ij}, \end{aligned} \quad (2.9)$$

$$\begin{aligned} \partial_t \tilde{\Gamma}^i = & -2\partial_j \alpha \tilde{A}^{ij} + 2\alpha \left[ \tilde{\Gamma}_{jk}^i \tilde{A}^{jk} - \frac{2}{3} \tilde{\gamma}^{ij} \partial_j K + 6\tilde{A}^{ij} \partial_j \phi \right] \\ & + \tilde{\gamma}^{jk} \partial_j \partial_k \beta^i + \frac{1}{3} \tilde{\gamma}^{ij} \partial_j \partial_k \beta^k + \beta^j \partial_j \tilde{\Gamma}^i - \tilde{\Gamma}^j \partial_j \beta^i + \frac{2}{3} \tilde{\Gamma}^i \partial_j \beta^j, \end{aligned} \quad (2.10)$$

where  $D_i$  is the covariant derivative with respect to the 3-metric  $\gamma_{ij}$  and TF means trace-free operation, i.e.,  $H_{ij}^{\text{TF}} = H_{ij} - \frac{1}{3} \gamma_{ij} H^k_k$ . The Ricci tensor is computed with the conformal connection  $\tilde{\Gamma}^i$  as

$$R_{ij} = R_{ij}^\phi + \tilde{R}_{ij}, \quad (2.11)$$

$$R_{ij}^\phi = -2\tilde{D}_i \tilde{D}_j \phi - 2\tilde{\gamma}_{ij} \tilde{D}^k \tilde{D}_k \phi + 4\tilde{D}_i \phi \tilde{D}_j \phi - 4\tilde{\gamma}_{ij} \tilde{D}^k \phi \tilde{D}_k \phi \quad (2.12)$$

$$\tilde{R}_{ij} = -\frac{1}{2} \tilde{\gamma}^{lk} \partial_k \partial_l \tilde{\gamma}_{ij} + \tilde{\gamma}_{k(i} \partial_j) \tilde{\Gamma}^k + \tilde{\gamma}^{lm} \tilde{\Gamma}_{lm}^k \tilde{\Gamma}_{(ij)k} + 2\tilde{\gamma}^{lm} \tilde{\Gamma}_{l(i} \tilde{\Gamma}_{j)km} + \tilde{\gamma}^{lm} \tilde{\Gamma}_{im}^k \tilde{\Gamma}_{klj}, \quad (2.13)$$

where  $\tilde{D}_i$  is a covariant derivative associated with  $\tilde{\gamma}_{ij}$ .

Similarly to the ADM formulation, this system has constraint equations. The two ‘‘kinematic’’ constraints,

the Hamiltonian and momentum constraint equations, are expressed in terms of the BSSN basic variables and are written as

$$\mathcal{H} = e^{-4\phi}\tilde{R} - 8e^{-4\phi}(\tilde{D}^i\tilde{D}_i\phi + \tilde{D}^i\phi\tilde{D}_i\phi) + \frac{2}{3}K^2 - \tilde{A}_{ij}\tilde{A}^{ij} - \frac{2}{3}\mathcal{A}K \approx 0, \quad (2.14)$$

$$\mathcal{M}_i = 6\tilde{A}^j{}_i\tilde{D}_j\phi - 2\mathcal{A}\tilde{D}_i\phi - \frac{2}{3}\tilde{D}_iK + \tilde{D}_j\tilde{A}^j{}_i \approx 0. \quad (2.15)$$

Additionally, the BSSN formulation requires three ‘‘algebraic’’ constraint relations;

$$\mathcal{G}^i = \tilde{\Gamma}^i - \tilde{\gamma}^{jk}\tilde{\Gamma}^i_{jk} \approx 0, \quad (2.16)$$

$$\mathcal{A} = \tilde{A}_{ij}\tilde{\gamma}^{ij} \approx 0, \quad (2.17)$$

$$\mathcal{S} = \tilde{\gamma} - 1 \approx 0, \quad (2.18)$$

where (2.16) and (2.17) are from the definitions of (2.5) and (2.4), respectively. Equation (2.18) is from the requirement on  $\tilde{\gamma}$ .

These five constraints are, theoretically, supposed to be zero at all times; therefore they can be used to modify the dynamical equations. For example, Alcubierre et al. [34] announced that the replacement of the terms in (2.10) using the momentum constraint drastically changes the stability feature. Actually, such replacements of terms using constraints are applied (with/without intentions) in many terms in (2.6)-(2.10), which are expressed as Eqs. (2.27)-(2.31) in [26].

Alcubierre et al. [35] also pointed out that the redefinition of  $\tilde{A}_{ij}$  by

$$\tilde{A}_{ij} \rightarrow \tilde{A}_{ij} - \frac{1}{3}\tilde{\gamma}_{ij}\text{tr}\tilde{A} \quad (2.19)$$

during the time evolutions improves the numerical stability. This technique again can be understood as the trace-out of the  $\mathcal{A}$ -constraint (2.17) from the evolution equations. In our numerical code, we do not apply this technique because we recognize the trace-free property as the new constraint  $\mathcal{A}$  in the BSSN system, and our purpose is to construct a system preventing the violation of constraints.

Recently, several groups applied artificial dissipation (e.g. [36]) to obtain stable evolutions (see, e.g. [32, 33, 37]). We, however, do not introduce such dissipations in our code, since we try to clarify the difference of stability from the viewpoint of *formulations* of the Einstein equations.

## B. Adjusted BSSN systems

To understand the stability property of the BSSN system, Yoneda and Shinkai [26] studied the structure of the evolution equations, (2.6)-(2.10), in detail, especially how the modifications using the constraints, (2.14)-(2.18), affect to the stability. They investigated the signature of the eigenvalues of the constraint propagation equations (dynamical equations of constraints), and explained that

the standard BSSN dynamical equations are balanced from the viewpoints of constrained propagations, including a clarification of the effect of the replacement using the momentum constraint equation.

Moreover, they predicted that several combinations of modifications have a constraint-damping nature, and named them *adjusted* BSSN systems. (Their predictions are based on the signature of eigenvalues of the constraint propagations, and the negative signature implies a dynamical system which evolves toward the constraint surface as the attractor.)

Among them, in this work, we test the following three adjustments:

1. An adjustment of the  $\tilde{A}$ -equation with the momentum constraint:

$$\partial_t\tilde{A}_{ij} = \partial_t^B\tilde{A}_{ij} + \kappa_A\alpha\tilde{D}_{(i}\mathcal{M}_{j)}, \quad (2.20)$$

where  $\kappa_A$  is predicted (from the eigenvalue analysis) to be positive in order to damp the constraint violations.

2. An adjustment of the  $\tilde{\gamma}$ -equation with  $\mathcal{G}$  constraint:

$$\partial_t\tilde{\gamma}_{ij} = \partial_t^B\tilde{\gamma}_{ij} + \kappa_{\tilde{\gamma}}\alpha\tilde{\gamma}_{k(i}\tilde{D}_{j)}\mathcal{G}^k, \quad (2.21)$$

with  $\kappa_{\tilde{\gamma}} < 0$ .

3. An adjustment of the  $\tilde{\Gamma}$ -equation with  $\mathcal{G}$  constraint:

$$\partial_t\tilde{\Gamma}^i = \partial_t^B\tilde{\Gamma}^i + \kappa_{\tilde{\Gamma}}\alpha\mathcal{G}^i. \quad (2.22)$$

with  $\kappa_{\tilde{\Gamma}} < 0$ .

These three adjustments are chosen as samples of ‘‘best candidates’’, Eq. (4.9)-(4.11) in [26]. The term ‘‘best’’ comes from their conjecture on the eigenvalue analysis of the constraint propagation matrix; that is, (a) all the resultant eigenvalues from above adjustments can be less than or at most equal to zero, which indicates the decay of constraint errors, and (b) the resultant constraint propagation matrix is diagonalizable, which guarantees the predictions of above eigenvalue analysis (see Table II in [26]). However, since above eigenvalues include zero elements and also above analysis assumes a linearly perturbed metric about the flat space-time, the effects of the adjustments (2.20)-(2.22) need to be demonstrated via numerical experiments.

### III. NUMERICAL TESTBED MODELS

Following the proposals of the Mexico Numerical Relativity Workshop [29], we perform three kinds of tests. In this section, we explicitly give some details of the models.

#### A. Gauge-wave testbed

The first test is the trivial Minkowski space-time, but sliced with the time-dependent 3-metric, which is called the gauge-wave test. The 4-metric is obtained by coordinate transformation from the Minkowski metric as

$$ds^2 = -Hdt^2 + Hdx^2 + dy^2 + dz^2, \quad (3.1)$$

where

$$H = H(x-t) = 1 - A \sin\left(\frac{2\pi(x-t)}{d}\right), \quad (3.2)$$

which describes a sinusoidal gauge wave of amplitude  $A$  propagating along the  $x$ -axis. The non-trivial extrinsic curvature is

$$K_{xx} = -\frac{\pi A}{d} \frac{\cos\left(\frac{2\pi(x-t)}{d}\right)}{\sqrt{1 + A \sin\frac{2\pi(x-t)}{d}}}. \quad (3.3)$$

Following [29], we chose numerical domain and parameters as follows:

- Gauge-wave parameters:  $d = 1$  and  $A = 10^{-2}$
- Simulation domain:  $x \in [-0.5, 0.5]$ ,  $y = z = 0$
- Grid:  $x^i = -0.5 + (n - \frac{1}{2})dx$  with  $n = 1, \dots, 50\rho$ , where  $dx = 1/(50\rho)$  with  $\rho = 2, 4, 8$
- Time step:  $dt = 0.25dx$
- Boundary conditions: Periodic boundary condition in  $x$  direction and planar symmetry in  $y$  and  $z$  directions
- Gauge conditions:

$$\partial_t \alpha = -\alpha^2 K, \quad \beta^i = 0. \quad (3.4)$$

The 1D simulation is carried out for a  $T = 1000$  crossing-time or until the code crashes, where one crossing-time is defined by the length of the simulation domain.

#### B. Linear wave testbed

The second test is to check the ability of handling a travelling gravitational wave. The initial 3-metric and extrinsic curvature  $K_{ij}$  are given by a diagonal perturbation with component

$$ds^2 = -dt^2 + dx^2 + (1+b)dy^2 + (1-b)dz^2, \quad (3.5)$$

where

$$b = A \sin\left(\frac{2\pi(x-t)}{d}\right) \quad (3.6)$$

for a linearized plane wave traveling in the  $x$ -direction. Here  $d$  is the linear size of the propagation domain and  $A$  is the amplitude of the wave. The non-trivial components of extrinsic curvature are then

$$K_{yy} = -\frac{1}{2}\partial_t b, \quad K_{zz} = \frac{1}{2}\partial_t b. \quad (3.7)$$

Following [29], we chose the following parameters:

- Linear wave parameters:  $d = 1$  and  $A = 10^{-8}$
- Simulation domain:  $x \in [-0.5, 0.5]$ ,  $y = 0$ ,  $z = 0$
- Grid:  $x^i = -0.5 + (n - \frac{1}{2})dx$  with  $n = 1, \dots, 50\rho$ , where  $dx = 1/(50\rho)$  with  $\rho = 2, 4, 8$
- Time step:  $dt = 0.25dx$
- Boundary conditions: Periodic boundary condition in  $x$  direction and planar symmetry in  $y$  and  $z$  directions
- Gauge conditions:  $\alpha = 1$  and  $\beta^i = 0$

The 1D simulation is carried out for a  $T = 1000$  crossing-time or until the code crashes.

#### C. Collapsing polarized Gowdy-wave testbed

The third test is to check the formulation in a strong field context using the polarized Gowdy metric, which is written as

$$ds^2 = t^{-1/2}e^{\lambda/2}(-dt^2 + dz^2) + t(e^P dx^2 + e^{-P} dy^2) \quad (3.8)$$

Here time coordinate  $t$  is chosen such that time increases as the universe expands. Simple forms of the solutions,  $P$  and  $\lambda$ , are given by

$$\begin{aligned} P &= J_0(2\pi t) \cos(2\pi z), \\ \lambda &= -2\pi t J_0(2\pi t) J_1(2\pi t) \cos^2(2\pi z) \\ &\quad + 2\pi^2 t^2 [J_0^2(2\pi t) + J_1^2(2\pi t)] \\ &\quad - \frac{1}{2} [(2\pi)^2 [J_0^2(2\pi) + J_1^2(2\pi)] \\ &\quad - 2\pi J_0(2\pi) J_1(2\pi)], \end{aligned} \quad (3.10)$$

where  $J_n$  is the Bessel function. The non-trivial extrinsic curvatures are then

$$K_{xx} = -\frac{1}{2} t^{1/4} e^{-\lambda/4} e^P (1 + tP_{,t}), \quad (3.11)$$

$$K_{yy} = -\frac{1}{2} t^{1/4} e^{-\lambda/4} e^{-P} (1 - tP_{,t}), \quad (3.12)$$

$$K_{zz} = \frac{1}{4} t^{-1/4} e^{\lambda/4} (t^{-1} - \lambda_{,t}). \quad (3.13)$$

According to [29], the new time coordinate  $\tau$ , which satisfies harmonic condition, is obtained by coordinate transformation as

$$t(\tau) = ke^{c\tau}, \quad (3.14)$$

where  $c$  and  $k$  are arbitrary constants. Using this freedom, we can set the lapse function in the new time coordinate to be unity at the initial time. Concretely, we set

$$\begin{aligned} t_0 = \tau_0 &\sim 9.8753205829098, \\ c &\sim 0.0021195119214617, \\ k &\sim 9.6707698127638, \end{aligned} \quad (3.15)$$

where  $t_0$  is the initial time. Following [29], we perform our evolution in the collapsing (i.e. backward in time) direction. Parameters are chosen as follows:

- Simulation domain:  $z \in [-0.5, 0.5]$ ,  $x = y = 0$
- Grid:  $z = -0.5 + (n - \frac{1}{2})dz$  with  $n = 1, \dots, 50\rho$ , where  $dz = 1/(50\rho)$  with  $\rho = 2, 4, 8$
- Time step:  $dt = 0.25dz$
- Boundary conditions: Periodic boundary condition in  $z$ -direction and plane symmetry in  $x$ - and  $y$ -directions
- Gauge conditions: the harmonic slicing (3.4) and  $\beta^i = 0$

The 1D simulation is carried out for a  $T = 1000$  crossing-time or until the code crashes.

## IV. THE CODE

### A. Code description

We have developed a new numerical code based on the adjusted BSSN systems. The variables are  $(\phi, \tilde{\gamma}_{ij}, K, A_{ij}, \tilde{\Gamma}^i)$ , and the evolution equations are (2.6)-(2.10) with/without adjustment (2.20), (2.21), and/or (2.22). The time-integration is under the free-evolution scheme, and we monitor five constraints, (2.14)-(2.18), to check the accuracy and stability of the evolutions.

Our time-integration scheme is the three-step iterative Crank-Nicholson method with centered finite difference in space [39]. This scheme should have second-order convergence both in space and time, and we checked its convergence in all the testbeds.

As we have already mentioned in the end of §II A, we do not apply the trace-out technique of  $\tilde{A}_{ij}$ , (2.19) in our code.

We also remark on our treatment of the conformal connection variable  $\tilde{\Gamma}^i$ . As was pointed out in [38], it is better not to use  $\tilde{\Gamma}^i$  in all the evolution equations. We surmise this is because the amplification of the error due to the

discrepancy of the definition (2.5), i.e., the accumulations of the violations of  $\mathcal{G}^i$ -constraint (2.16). Therefore, we used the evolved  $\tilde{\Gamma}^i$  only for the terms in (2.10) and (2.13), and not for other terms, so as not to implicitly apply the  $\mathcal{G}^i$ -constraint in time evolutions.

### B. Debugging procedures

It is crucial that our code can produce accurate results, because the adjustment methods are based on the assumption that the code represents the BSSN system (2.6)-(2.10) accurately. We verified our code by comparing our numerical data with analytic solutions from the gauge-wave and Gowdy-wave testbeds in Sec. III. The actual procedures are as follows:

1. Evolve only one component, e.g.  $\tilde{A}_{xx}$ , numerically, and express all the other components with those of the analytic solution. In this situation, the origin of the error is from the finite differencing of the analytic solution in the spatial direction and from that of the numerically evolved component ( $\tilde{A}_{xx}$ ) both in spatial and time directions. We checked the code by monitoring the difference between the numerically evolved component ( $\tilde{A}_{xx}$ ) and its analytic expression. This procedure was applied to all the components one by one.
2. Evolve only several components, e.g.,  $\tilde{A}_{xx}$  and  $\tilde{\Gamma}^x$ , numerically, and express the other components by the analytic solution. The error can be checked by a procedure similar to the one above.
3. Evolve all the components numerically, and check the error with the analytic solution.

We repeated these procedure three times by switching the propagation directions ( $x$ ,  $y$ , and  $z$ -directions) of gauge-wave and Gowdy-wave solutions. We also applied these procedures in a 2D test [29], and checked the off-diagonal component.

### C. Error evaluation methods

It should be emphasized that the adjustment effect has two meanings, improvement of stability and of accuracy. Even if a simulation is stable, it does not imply that the result is accurate. We judge the stability of the evolution by monitoring the L2 norm of each constraint,

$$\|\delta\mathcal{C}\|_2(t) \equiv \sqrt{\frac{1}{N} \sum_{x,y,z} (\mathcal{C}(t; x, y, z))^2}, \quad (4.1)$$

where  $N$  is the total number of grid points, while we judge the accuracy by the difference of the metric components  $g_{ij}(t; x, y, z)$  from the exact solution

$$g_{ij}^{(\text{exact})}(t; x, y, z),$$

$$\|\delta g_{ij}\|_2(t) \equiv \sqrt{\frac{1}{N} \sum_{x,y,z} \left( g_{ij} - g_{ij}^{(\text{exact})} \right)^2}. \quad (4.2)$$

#### D. Magnitude of $\kappa$

Adjusted systems, (2.20)-(2.22), require to specify the parameter  $\kappa$ . From the analytical prediction in [26] we know the signature of  $\kappa$ , but not for its magnitude. By definition of the adjustment terms in Eq. (2.20)-(2.22), applying small  $\kappa$  should produce the close results with those of the plain system. On the contrary, the large  $\kappa$  system will violate the Courant-Friedrich-Lewy condition [40]. Hence, there exists a suitable region in the adjustment parameters.

At this moment, we have to chose  $\kappa$  experimentally, by observing the life-time of simulations. The value of  $\kappa$ , used in our demonstrations, is one of the choices of which the adjustment works effectively in all the resolutions.

### V. NUMERICAL RESULTS

#### A. Gauge-wave test

##### 1. The plain BSSN system

As the first test, we show the plain BSSN evolution (that is, no adjustments) in Fig. 1 for the gauge-wave test. In Fig. 1, the L2 norms of the Hamiltonian and momentum constraints (4.1) are plotted as a function of the crossing-time. The second-order convergent nature is lost at an early time, the 20 crossing-time, and the simulation crashes at about the 100 crossing-time. The poor performance of the plain BSSN system for the gauge wave test has been reported in [31] (see their Fig. 8). This drawback, on the other hand, can be overcome if one uses the fourth-order finite differencing scheme, an example of which can be seen in [32] (see their Fig. 2).

##### 2. Adjusted BSSN with $\tilde{A}$ -equation

We found that the simulation lasts 10 times longer with the adjustment in the  $\tilde{A}$ -equation using the momentum constraint (2.20). Figure 2 shows the L2 norms of the Hamiltonian and Momentum constraints in the same style as in Fig. 1. The adjustment parameter is set at  $\kappa_A = 0.005$  for this plot. We obtain almost perfect overlap of the rescaled Hamiltonian constraint for 200 crossing-times and almost perfect overlap in the momentum constraint for 50 crossing-times; there apparently improve the results of the plain BSSN system (see Fig. 1). We show the plots until the 1000 crossing-time, there we observe the growth of the error both in later time and in

higher resolution cases. However, it is also true that all errors are still under the errors of the plain BSSN system. Therefore, we conclude that this adjusted system shows a weaker instability than the plain system.

##### 3. Adjusted BSSN with $\tilde{\Gamma}$ -equation

The case of the adjustment of the  $\tilde{\Gamma}$ -equation using the  $\mathcal{G}$  constraint (2.22) is shown in Fig. 3.

The adjustment parameter is set at  $\kappa_{\tilde{\Gamma}} = -0.1$ . We find that the second-order convergence breaks down near the 40 crossing-time under the Momentum constraint, which is almost the same as with the plain BSSN system. However, the convergence of the Hamiltonian constraint is improved, i.e., it continues to the near 55 crossing-time. The life-time of the simulation is almost the same as that of the plain BSSN system.

##### 4. Adjusted BSSN with $\tilde{\gamma}$ -equation

We also tested the cases of the adjustment of the  $\tilde{\gamma}$ -equation using the  $\mathcal{G}$  constraint, (2.21). We again observed the effects of the adjustment on its stability and accuracy but found a rather small effect compared to the cases of the adjustments of (2.20) or (2.22), up to our trials of the parameter range of  $\kappa_{\tilde{\gamma}}$ . Therefore we omit showing the results.

##### 5. Evaluation of Accuracy

For evaluating the accuracy, we prepare Fig. 4(a), in which we plot the L2 norm of the error in  $\gamma_{xx}$ , (4.2), with the function of time. Three lines correspond to the result of the plain BSSN system,  $\tilde{A}$ -eq. adjusted, and  $\tilde{\Gamma}$ -eq. adjusted BSSN system, respectively. The  $\tilde{\Gamma}$ -adjustment makes the life-time slightly longer than that of the plain BSSN, while  $\tilde{A}$ -adjustment increases the life-time of the simulation by a factor of 10. However, it is also true that the error grows in time in all the three cases.

We also find that the error is induced by distortion of the wave, i.e. the both phase and amplitude errors distort the numerical solution. In Fig. 4(b), we show a snapshot of  $\gamma_{xx}$  numerical solution at  $T = 100$ , together with the exact solution at the same time coordinate. The amplitude difference between the numerical and exact solutions is apparently less when we use the  $\tilde{A}$ -eq. adjusted system than that of the plain system. In Sec. VI later, we discuss what causes the error and why the simulation life-time becomes longer when we use the adjusted system.

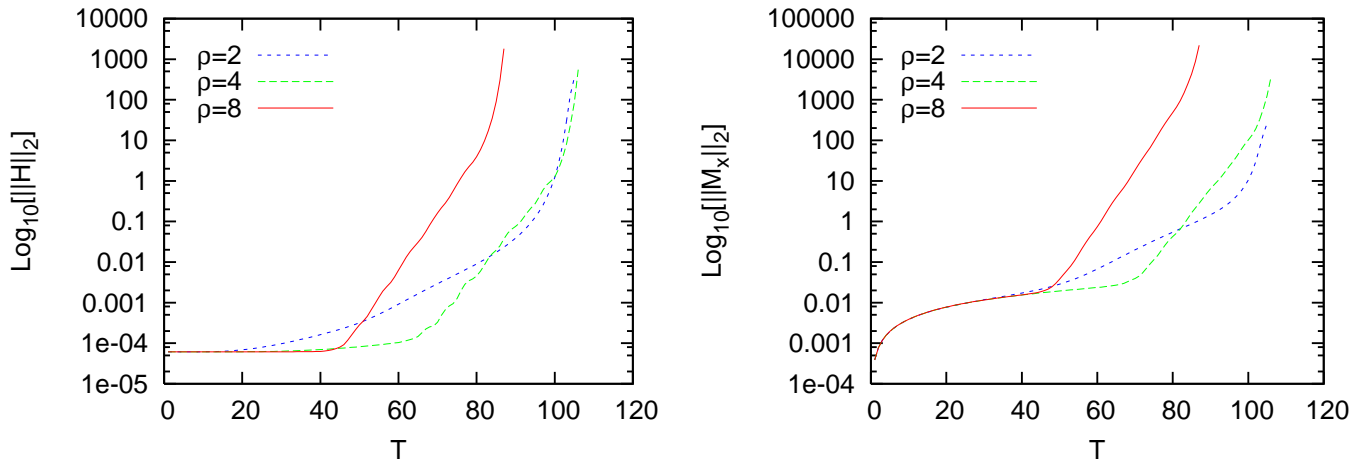


FIG. 1: The one-dimensional gauge-wave test with the plain BSSN system. The L2 norm of  $\mathcal{H}$  and  $\mathcal{M}_x$ , rescaled by  $\rho^2/4$ , are plotted with a function of the crossing-time. The amplitude of the wave is  $A = 0.01$ . The loss of convergence at the early time, near the 20 crossing-time, can be seen, and it will produce the blow-ups of the calculation in the end.

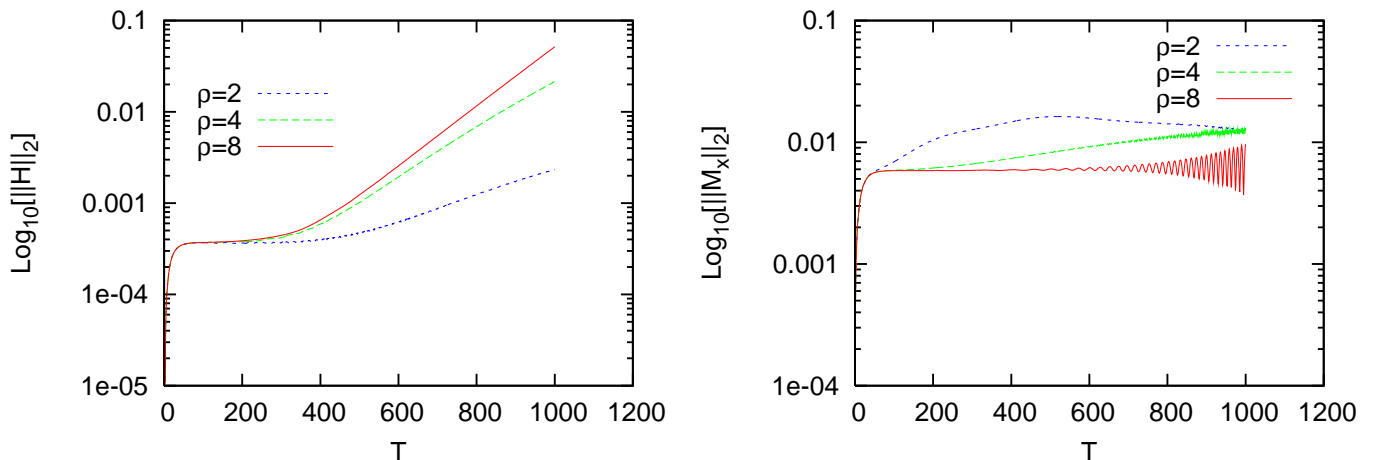


FIG. 2: The one-dimensional gauge-wave test with the adjusted BSSN system in the  $\tilde{A}$ -equation (2.20). The L2 norm of  $\mathcal{H}$  and  $\mathcal{M}_x$ , rescaled by  $\rho^2/4$ , are plotted with a function of the crossing-time. The wave parameter is the same as with Fig. 1, and the adjustment parameter  $\kappa_A$  is set to  $\kappa_A = 0.005$ . We see the higher resolution runs show convergence longer, i.e., the 300 crossing-time in  $\mathcal{H}$  and the 200 crossing-time in  $\mathcal{M}_x$  with  $\rho = 4$  and 8 runs. All runs can stably evolve up to the 1000 crossing-time.

### B. Linear wave test

The second test is the linear wave propagation test, §III B, to check the accuracy of wave propagations in the adjusted systems. We find that the linear wave testbed

does not produce a significant constraint violation even for the plain BSSN system. The simulation does not crash at the 1000 crossing-time irrespective of the resolutions. Figure 5 illustrates the profiles of  $\gamma_{zz} - 1$  at the 500 crossing-time. The figure indicates the simulation does not produce the amplitude error but does pro-

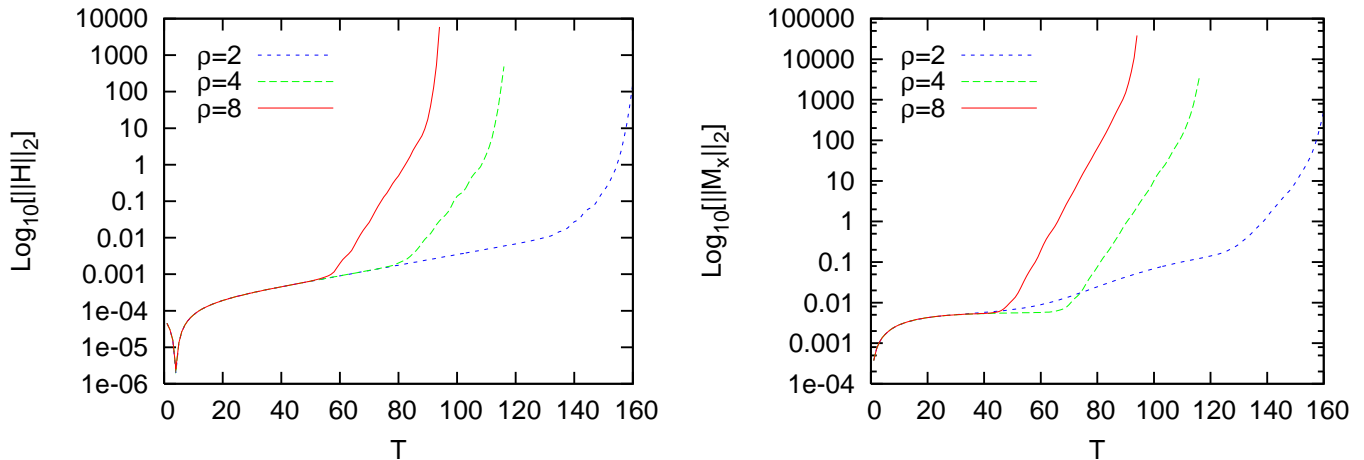


FIG. 3: The one-dimensional gauge-wave test with the adjusted BSSN system in the  $\tilde{\Gamma}$ -equation (2.22). The L2 norm of  $\mathcal{H}$  and  $\mathcal{M}_x$ , rescaled by  $\rho^2/4$ , are plotted with a function of the crossing-time. The wave parameter is the same as Fig. 1, and the adjustment parameter is  $\kappa_{\tilde{\Gamma}} = -0.1$ . Note the near perfect overlap for the 55 crossing-time in  $\mathcal{H}$  and the 40 crossing-time in  $\mathcal{M}_x$ .

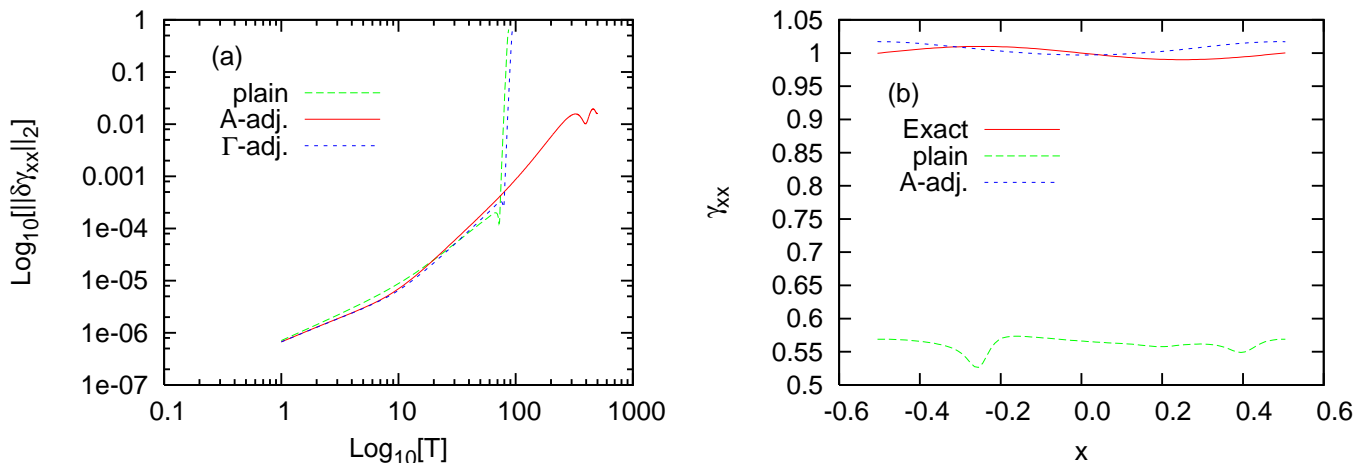


FIG. 4: Evaluation of the accuracy of the one-dimensional gauge-wave testbed. Lines show the plain BSSN, the adjusted BSSN with  $\mathcal{A}$ -equation, and with  $\tilde{\Gamma}$ -equation. (a) The L2 norm of the error in  $\gamma_{xx}$ , using (4.2). (b) A snapshot of the exact and numerical solution at  $T = 100$ .

duce the phase error. However, we also observe that the higher resolution run reduces the phase error. We tried the same evolutions with adjusted BSSN systems. However, all the results are indistinguishable from the those of the plain BSSN system. This is because the adjusted terms of the equations are small due to the small violations of constraints. Figure 6 shows a snapshot of the error defined by  $\gamma_{zz} - \gamma_{zz}^{(\text{exact})}$  at the 500 crossing-time both for the plain BSSN system and the adjusted BSSN system where the  $\tilde{A}$ -equation where  $\kappa_{\mathcal{A}} = 10^{-3}$ . Since

two lines are matching quite well, we can say that the adjusted BSSN system produces the same result as the plain BSSN system, including the phase error. Results from the other adjusted BSSN systems are almost the same qualitatively, including their convergence features. We also remark that we do not see a case in which adjustment worsens accuracy and stability.

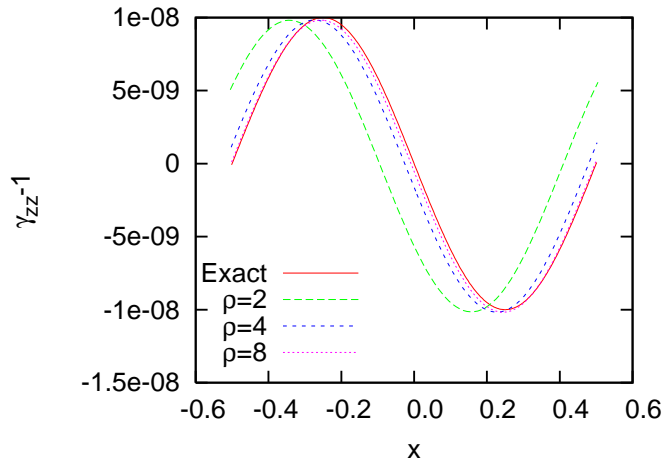


FIG. 5: Snapshots of the one-dimensional linear wave at different resolutions with the plain BSSN system at the simulation time 500 crossing-time. We see there exists phase error, but they are convergent away at higher resolution runs.

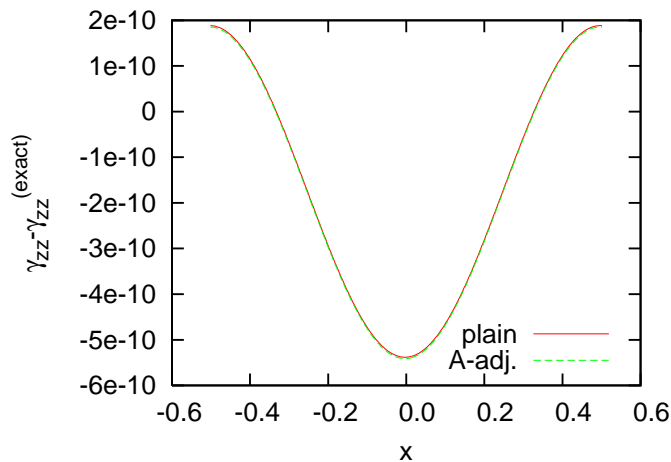


FIG. 6: Snapshot of errors with the exact solution for the Linear Wave testbed with the plain BSSN system and the adjusted BSSN system with the  $\tilde{A}$  equation at  $T = 500$ . The highest resolution  $\rho = 8$  is used in both runs. The difference between the plain and the adjusted BSSN system with the  $\tilde{A}$  equation is indistinguishable. Note that the maximum amplitude is set to be  $10^{-8}$  in this problem.

### C. Gowdy-wave test

The third test is the polarized Gowdy-wave test, §III C, to check the adjustments in the strong field regime.

#### 1. The plain BSSN

In Fig. 7, We first show the case of the plain BSSN evolution. We find that the second-order convergence continues up-to the 100 crossing-time and the higher resolutions runs tend to crash at early times. This behavior (and crashing time) almost coincides with the results of the *Cactus* BSSN code, reported by Alcubierre et al. [29] (see their Fig. 7). (We remark that Zlochower et al. [32]

reported they can produce the stable and accurate evolution for the 1000 crossing-time by implementing the higher order differencing scheme to their *LazEv* code. However, it should be emphasized that they suggested their code produces the stable simulation only when they used the Kreiss-Oliger dissipation term [36].)

#### 2. Adjusted BSSN with $\tilde{A}$ -equation

Adjustment of the  $\tilde{A}$ -equation using the momentum constraint (2.20), extends the life-time of the simulation 10 times longer for the highest resolution run. Figure 8 depicts the rescaled L2 norm of  $\mathcal{H}$  and  $\mathcal{M}_z$  versus time. We set  $\kappa_{\mathcal{A}} = -0.001$ . (Note that the signature of  $\kappa$  is

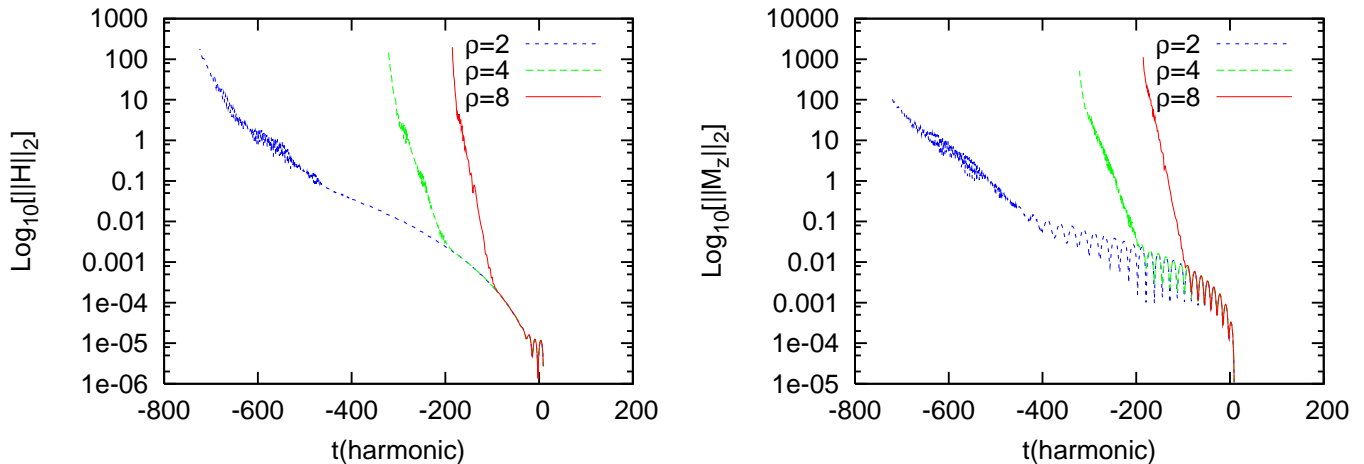


FIG. 7: Collapsing polarized Gowdy-wave test with the plain BSSN system. The L2 norm of  $\mathcal{H}$  and  $\mathcal{M}_z$ , rescaled by  $\rho^2/4$ , are plotted with a function of the crossing-time. (Simulation proceeds backwards from  $t = 0$ .) We see almost perfect overlap for the initial 100 crossing-time, and the higher resolution runs crash earlier. This result is quite similar to those achieved with the Cactus BSSN code, reported by [29].

reversed from the expected one, since the evolution is backward in time.)

We find that an almost perfect overlap up to the 1000 crossing-time under both the Hamiltonian constraint and the Momentum constraint. (These overlaps indicate that the error in  $\mathcal{H}$  and  $\mathcal{M}_z$  in the  $\rho = 8$  resolution runs are 16 times smaller than these errors in the  $\rho = 2$  resolution run. ) However, we also find oscillations in the Momentum constraint, especially in the end of the simulation.

### 3. Adjusted BSSN with $\tilde{\gamma}$ -equation

The case of the adjustment of the  $\tilde{\gamma}$ -equation using the  $\mathcal{G}$ -constraint (2.21), is shown in Fig. 9. The adjustment parameter  $\kappa_{\tilde{\gamma}}$  is set at 0.000025. (Again, the signature of  $\kappa$  is reversed from the expected one.)

Figure 9 shows that an almost perfect overlap is obtained for the 200 crossing-time in both  $\mathcal{H}$  and  $\mathcal{M}_z$ . The higher resolution runs tend to crash at earlier times, which is same as with the plain BSSN system. However, the convergence time becomes longer than that of the plain BSSN system. We will discuss the quantitative improvement for the  $\tilde{\gamma}$ -adjustment in the next subsection.

### 4. Adjustment effect

In order to check the *accuracy* of the simulations, we prepare Fig. 10 to show the error of the  $\gamma_{zz}$  component

of the metric.

Unlike the gauge-wave or the linear wave test, in this Gowdy-wave test the amplitude of the metric functions damps with time. Therefore we use the criterion that the error normalized by  $\gamma_{zz}$  be under 1% for an *accurate evolution*. This criterion is the same as the one used in Zlochower et al. [32].

Figure 10 shows the normalized error in  $\gamma_{zz}$  versus time for the plain BSSN, adjusted BSSN with  $\mathcal{A}$ -equation, and adjusted BSSN with  $\tilde{\gamma}$ -equation systems. We find that these three systems produce accurate results up to  $t = 200$ ,  $t = 1000$ , and  $t = 400$ , respectively. This proves that the adjustments work effectively, i.e, they make possible a stable and accurate simulation, especially the  $\mathcal{A}$ -adjusted BSSN system.

## VI. SUMMARY AND DISCUSSION

In this article, we presented our numerical comparisons of the BSSN formulation and its adjusted versions using constraints. We performed three testbeds: gauge-wave, linear wave, and collapsing polarized Gowdy-wave tests with their evolutions by three kinds of adjustments, which were previously proposed by Yoneda and Shinkai [26] based on their constraint propagation analysis.

The idea of the adjusted systems is to construct a system robust against constraint violations by modifying the evolution equations using the constraint equations.

We can summarize our tests as follows:

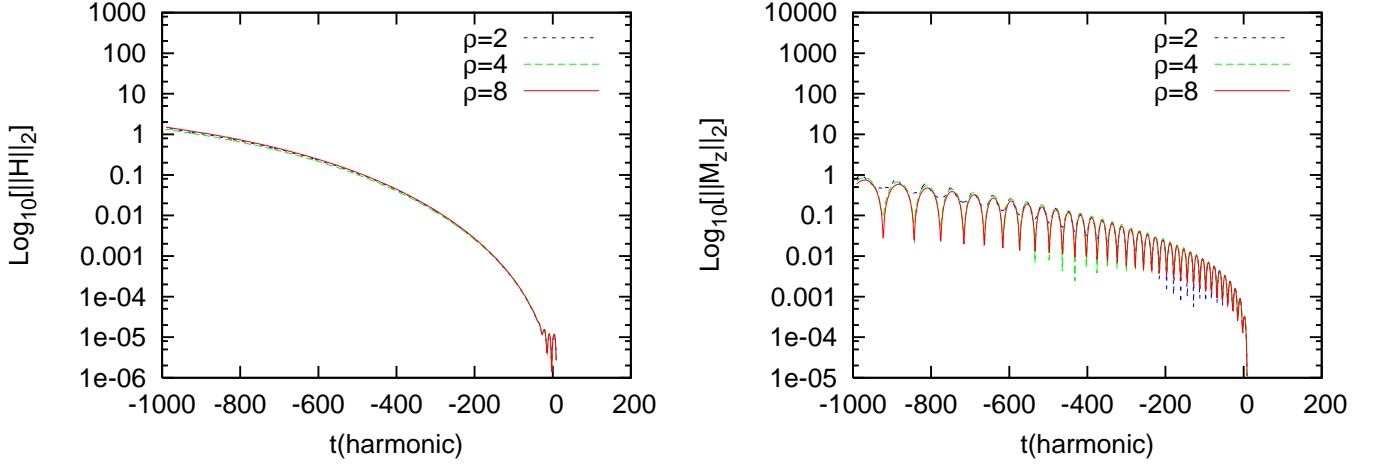


FIG. 8: Collapsing polarized Gowdy-wave test with the adjusted BSSN system in the  $\tilde{A}$ -equation (2.20), with  $\kappa_A = -0.001$ . The style is the same as in Fig. 7 and note that both constraints are normalized by  $\rho^2/4$ . We see almost perfect overlap for the initial 1000 crossing-time in both constraint equations,  $\mathcal{H}$  and  $\mathcal{M}_z$ , even for the highest resolution run.

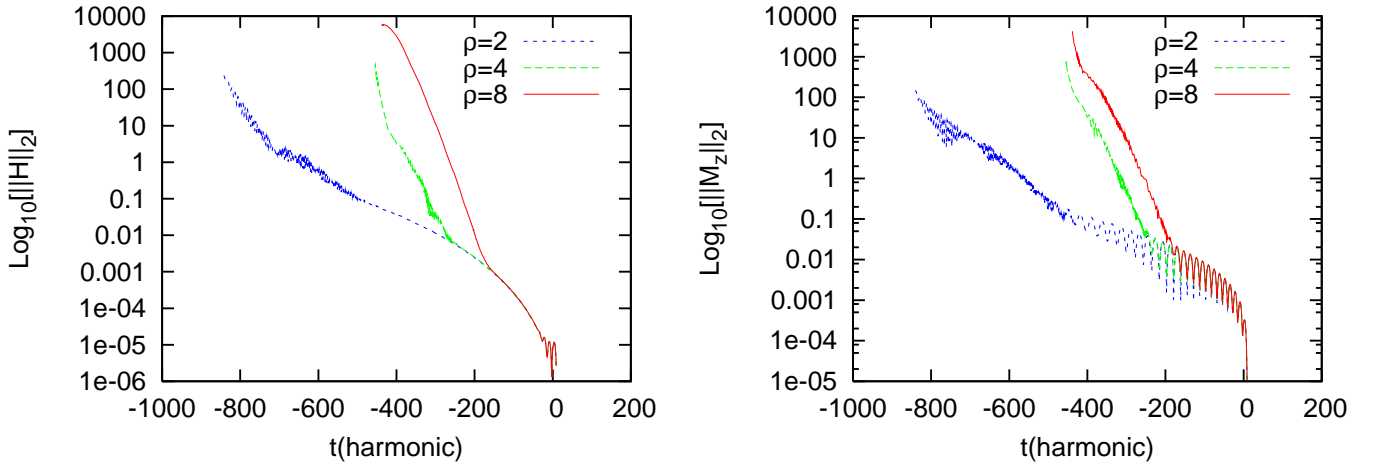


FIG. 9: Collapsing polarized Gowdy-wave test with the adjusted BSSN system in the  $\tilde{\gamma}$ -equation (2.21), with  $\kappa_{\tilde{\gamma}} = 0.000025$ . The figure style is the same as Figure 7. Note the almost perfect overlap for 200 crossing-time in the both the Hamiltonian and Momentum constraint and the  $\rho = 2$  run can evolve stably for 1000 crossing-time.

- When the plain (original) BSSN evolutions already show satisfactory good evolutions (e.g., the linear wave test), the constraint violations (i.e., adjusted terms) are also small or ignorable.

Therefore the adjusted BSSN equations become quite similar to the plain BSSN equations, and their results coincide with the plain BSSN results.

- Among the adjustments we tried, we observed that the adjusted BSSN system with the  $\tilde{A}$ -eq. (2.20) is the most robust for all the testbeds examined in this study. It gives us an accurate and stable evolution compared to the plain BSSN system. Quantitatively, the life-time of the simulation becomes 10 times longer for the gauge-wave testbed and 5 times longer for the Gowdy-wave testbed than the

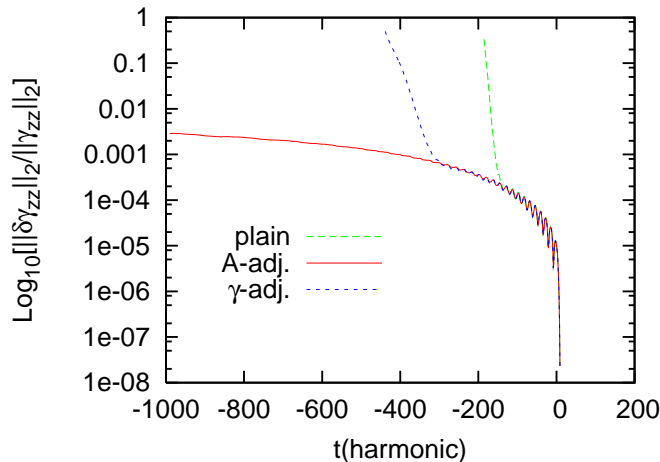


FIG. 10: Comparisons of systems in the collapsing polarized Gowdy-wave test. The L2 norm of the error in  $\gamma_{zz}$ , rescaled by the L2 norm of  $\gamma_{zz}$ , for the plain BSSN, adjusted BSSN with  $\tilde{A}$ -equation, and with  $\tilde{\gamma}$ -equation are shown. The highest resolution run,  $\rho = 8$ , is depicted for the plots. We can conclude that the adjustments make longer accurate runs available. Note that the evolution is backwards in time.

life-time of the plain BSSN system. However, it should be noted that for the gauge-wave testbed, the convergence feature is lost at a comparatively early time, the 200 crossing-time in the Hamiltonian constraint and the 50 crossing-time in the momentum constraint.

Recently, it has been claimed that the set up of the gauge wave problem in Apples-with-Apples has a problematic point [37], which arises from the harmonic gauge condition. In [41], it is argued that this gauge has a residual freedom in the form  $H \rightarrow e^{\lambda t} H$ , where  $\lambda$  is an arbitrary and  $H$  is a function in Eq. (3.1). Of course, our set up corresponds to the  $\lambda = 0$  case, but numerical error easily excites modes that result in either exponentially increasing or decaying metric amplitude. Actually, we find the amplitude of the error decays with time in this testbed. So, we conclude that due to the adjustment, the growing rate of the gauge mode is suppressed and the life-time of the simulation is extended as a result.

- The other type of adjustments (2.21 and 2.22) show their apparent effects while depending on a problem. The  $\tilde{\Gamma}$ -adjustment for the gauge-wave testbed makes the life-time longer slightly. The  $\tilde{\gamma}$ -adjustment for the Gowdy-wave testbed makes possible a simulation twice as long as the plain BSSN system.

We can understand the effect of the adjustments in terms of adding dissipative terms. By virtue of the definition of the constraints, we can recognize that the adjusted equation corresponds to the diffusion equation (see, for example, Eq. (2.20)) and the signature of  $\kappa$  determines whether the diffusion is positive or negative. In the adjusted  $\tilde{A}$ -eq. system, (2.20), the adjustment term corresponds to the positive diffusive term, due to the defini-

tion of  $\mathcal{M}_i$  and the positiveness of  $\kappa_A$  (see Eq. (2.15) and (2.20)). This fact might explain why the adjusted  $\tilde{A}$ -eq. system works effectively for all the testbeds.

In contrast, why are not all the adjustments effective in all testbeds? As we mentioned in Sec. IIB, the eigenvalue analysis was made on the linearly perturbed violation of constraints on the Minkowski space-time. Since the constraint violation grows non-linearly as seen in the Appendix of [26], the candidates may not be the best in their later evolution phase.

We remark upon two more interesting aspects arising from our study. The first is the mechanism of the constraint violations. As was shown in the appendix of [26], each constraint propagation (behavior of their growth or decrease) depends on the other constraint terms together with itself. That is, we can guess  $\mathcal{A}$  and  $\mathcal{S}$  constraints (2.17 and 2.18) in this article, propagate independently of the other constraints, while the violation of the  $\mathcal{G}$ -constraint, (2.16) is triggered by the violation of the momentum constraint, and both the Hamiltonian and the momentum constraints are affected by all the other constraints. Such an order of the constraint violation can be guessed in Fig. 11 (earlier time), where we plot the rate of constraint violation normalized with its initial value,  $||\delta\mathcal{C}||_2(t)/||\delta\mathcal{C}||_2(0)$ , as a function of time, for the gauge-wave testbeds with the plain BSSN evolution. (Note that the constraints at the initial time,  $\delta\mathcal{C}(0)$ , are not zero due to the numerical truncation error.) The parameters are the same as those shown in Sec. III A, and the lowest resolution run is used. From this investigation, we might conclude that to monitor the momentum constraint violation is the key to checking the stability of the evolution.

The second remark is on the Lagrange multipliers,  $\kappa$ , used in the adjusted systems. As discussed in Sec. IIB,

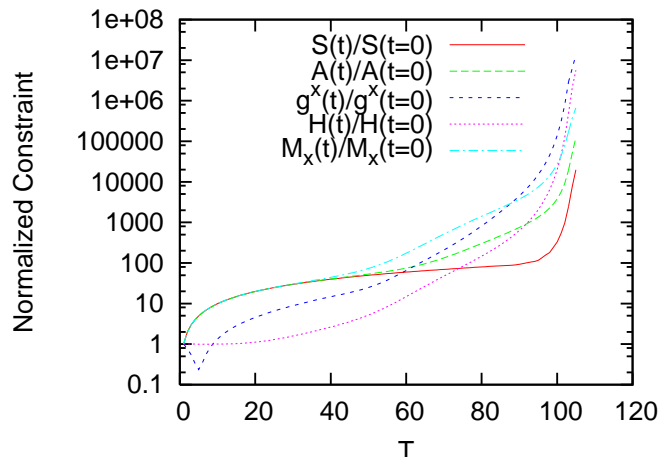


FIG. 11: The violation of all constraints normalized with their initial values,  $\|\delta\mathcal{C}\|_2(t)/\|\delta\mathcal{C}\|_2(0)$ , are plotted with a function of time. The evolutions of the gauge-wave testbeds with the plain BSSN system are shown. The parameters of the test are the same as those shown in Sec. III A, and the lowest resolution run,  $\rho = 2$ , is applied. By observing which constraint triggers the other constraint's violation from the constraint propagation equations, we may guess the mechanism by which the entire system is violating accuracy and stability. See the text for details.

the signatures of the  $\kappa$ s are determined *a priori*, and we confirmed that all the predicted signatures of  $\kappa$ s in [26] are right to produce positive effects for controlling constraint violations. However, we have to search for a suitable magnitude of  $\kappa$ s for each problem. Therefore we are now trying to develop a more sophisticated version, such as an auto-controlling  $\kappa$  system, which will be reported upon in the future elsewhere.

Although the testbeds used in this work are simple, it might be rather surprising to observe the expected effects of adjustments with such a slight change in the evolution equations. We therefore think that our demonstrations imply a potential to construct a robust system against constraint violations even in highly dynamical situations, such as black hole formation via gravitational collapse, or binary merger problems. We are now preparing our strong-field tests of the adjusted BSSN systems using large amplitude gravitational waves, black hole space-

time, or non-vacuum space-time, which will be reported on in the near future.

### Acknowledgments

K.K. thanks K. I. Maeda and S. Yamada for continuing encouragement. K.K. also thanks Y. Sekiguchi and M. Shibata for their useful comments on making numerical code. This work was supported in part by the Japan Society for Promotion of Science (JSPS) Research Fellowships and by a Grant-in-Aid for Scientific Programs. H.S. was partially supported by the Special Research Fund (Project No. 4244) of the Osaka Institute of Technology. A part of the numerical calculations was carried out on the Altix3700 BX2 at YITP at Kyoto University.

- 
- [1] M. Shibata, K. Taniguchi and K. Uryu, Phys. Rev. D **68**, 084020 (2003), Phys. Rev. D **71**, 084021 (2005)
  - [2] M. Shibata and K. Taniguchi, Phys. Rev. D **73**, 064027 (2006)
  - [3] P. Marronetti and S. L. Shapiro, Phys. Rev. D **68**, 104024 (2003)
  - [4] P. Marronetti, M. D. Duez, S. L. Shapiro and T. W. Baumgarte, Phys. Rev. Lett. **92**, 141101 (2004)
  - [5] J. A. Faber, T. W. Baumgarte, S. L. Shapiro and K. Taniguchi, Astrophys. J. **641**, L93 (2006)
  - [6] F. Pretorius, Phys. Rev. Lett. **95**, 121101 (2005)
  - [7] M. Campanelli, C. O. Lousto, P. Marronetti and Y. Zlochower, Phys. Rev. Lett. **96**, 111101 (2006)
  - [8] J. G. Baker, J. Centrella, D-I. Choi, M. Koppitz, J. van Meter, Phys. Rev. Lett. **96**, 111102 (2006).
  - [9] P. Diener, F. Herrmann, D. Pollney, E. Schnetter, E. Seidel, R. Takahashi, J. Thornburg, J. Ventrella, Phys. Rev. Lett. **96**, 121101 (2006)
  - [10] F. Herrmann, I. Hinder, D. Shoemaker, P. Laguna, gr-qc/0601026v2
  - [11] Z. B. Etienne, J. A. Faber, Y. T. Liu, S. L. Shapiro and T. W. Baumgarte, arXiv:0707.2083 [gr-qc].
  - [12] W. Tichy and P. Marronetti, Phys. Rev. D **76**, 061502 (2007)
  - [13] M. Campanelli, C. O. Lousto, Y. Zlochower and D. Merritt, Phys. Rev. Lett. **98**, 231102 (2007)
  - [14] J. A. Gonzalez, M. D. Hannam, U. Sperhake, B. Bruggmann and S. Husa, Phys. Rev. Lett. **98**, 231101 (2007)

- [15] M. Campanelli, C. O. Lousto, Y. Zlochower and D. Merritt, *Astrophys. J.* **659**, L5 (2007)
- [16] J. Thornburg, P. Diener, D. Pollney, L. Rezzolla, E. Schnetter, E. Seidel and R. Takahashi, *Class. Quant. Grav.* **24**, 3911 (2007)
- [17] J. A. Gonzalez, U. Sperhake, B. Bruegmann, M. Hannam and S. Husa, *Phys. Rev. Lett.* **98**, 091101 (2007)
- [18] J. G. Baker, J. Centrella, D. I. Choi, M. Koppitz and J. van Meter, *Phys. Rev. D* **73**, 104002 (2006)
- [19] M. Shibata and K. Uryu, *Phys. Rev. D* **74**, 121503 (2006), *Class. Quant. Grav.* **24**, S125 (2007)
- [20] T.W. Baumgarte and S.L. Shapiro, *Phys. Rev. D* **59**, 024007 (1999).
- [21] T. Nakamura, K. Oohara and Y. Kojima, *Prog. Theor. Phys. Suppl.* **90**, 1 (1987). M. Shibata and T. Nakamura, *Phys. Rev. D* **52**, 5428 (1995).
- [22] T. Nakamura, K. Oohara and Y. Kojima, *Prog. Theor. Phys. Suppl.* **90**, 1 (1987). T. Nakamura and K. Oohara, in *Frontiers in Numerical Relativity* edited by C.R. Evans, L.S. Finn, and D.W. Hobill (Cambridge Univ. Press, Cambridge, England, 1989).
- [23] H. Beyer, and O. Sarbach, *Phys. Rev. D* **70**, 104004 (2004).
- [24] C. Gundlach, J. M. Martin-Garcia, *Phys. Rev. D* **74**, 024016 (2006).
- [25] H. Shinkai and G. Yoneda, gr-qc/0209111.
- [26] G. Yoneda and H. Shinkai, *Phys. Rev. D* **66**, 124003 (2002).
- [27] H. Shinkai and G. Yoneda, *Class. Quant. Grav.* **19**, 1027 (2002).
- [28] H-J. Yo, T.W. Baumgarte and S.L. Shapiro, *Phys. Rev. D* **66**, 084026 (2002).
- [29] M. Alcubierre *et al.*, *Class. Quant. Grav.* **21**, 589 (2004)
- [30] M. Boyle, L. Lindblom, H. P. Pfeiffer, M.A. Scheel, and L. E. Kidder, *Phys. Rev. D* **75**, 024006 (2007)
- [31] N. Jansen, B. Bruegmann and W. Tichy, *Phys. Rev. D* **74**, 084022 (2006)
- [32] Y. Zlochower, J. G. Baker, M. Campanelli and C. O. Lousto, *Phys. Rev. D* **72**, 024021 (2005)
- [33] B. Bruegmann, J. A. Gonzalez, M. Hannam, S. Husa, U. Sperhake and W. Tichy, arXiv:gr-qc/0610128.
- [34] M. Alcubierre, G. Allen B. Brüggmann, E. Seidel and W.-M. Suen *Phys. Rev. D* **62**, 124011 (2000)
- [35] M. Alcubierre *et al.*, *Phys. Rev. D* **62**, 044034 (2000)
- [36] H. -O. Kreiss and J. Olinger, *Methods for Approximate Solution of Time Dependent Problems* (GARP Publication Series, Geneva, 1973).
- [37] M. C. Babiuc *et al.* [Apples With Apples Collaboration], arXiv:0709.3559 [gr-qc].
- [38] M. Alcubierre, B. Bruegmann, P. Diener, M. Koppitz, D. Pollney, E. Seidel and R. Takahashi, *Phys. Rev. D* **67**, 084023 (2003)
- [39] S. A. Teukolsky, *Phys. Rev. D* **61**, 087501 (2000)
- [40] G. Yoneda and H. Shinkai, *Class. Quant. Grav.* **18**, 441 (2001).
- [41] M. Babiuc, B. Szilagyi and J. Winicour, in *Nalytical and Numerical Approaches to Mathematical Relativity* eds. by J. Frauendiener, D. Giulini, and V. Perlick, (Springer, Heidelberg, 2006). [arXiv:gr-qc/0404092].
- [42] W. Press, B. P. Flannery, S. Teukolosky, and W. T. Vetterling, *Numerical Recipes in C* (Cambridge University Press, Cambridge, England, 1986).

# Numerical experiments of adjusted BSSN systems for controlling constraint violations

Kenta Kiuchi<sup>1</sup> \* and Hisa-aki Shinkai<sup>2</sup> †

<sup>1</sup>*Department of Physics, Waseda University, 3-4-1 Okubo, Shinjuku-ku, Tokyo 169-8555, Japan and*

<sup>2</sup>*Faculty of Information Science and Technology, Osaka Institute of Technology,  
1-79-1 Kitayama, Hirakata, Osaka 573-0196, Japan*

(Dated: December 24, 2018)

We present our numerical comparisons between the BSSN formulation widely used in numerical relativity today and its adjusted versions using constraints. We performed three testbeds: gauge-wave, linear wave, and Gowdy-wave tests, proposed by the Mexico workshop on the formulation problem of the Einstein equations. We tried three kinds of adjustments, which were previously proposed from the analysis of the constraint propagation equations, and investigated how they improve the accuracy and stability of evolutions. We observed that the signature of the proposed Lagrange multipliers are always right and the adjustments improve the convergence and stability of the simulations. When the original BSSN system already shows satisfactory good evolutions (e.g., linear wave test), the adjusted versions also coincide with those evolutions; while in some cases (e.g., gauge-wave or Gowdy-wave tests) the simulations using the adjusted systems last 10 times as long as those using the original BSSN equations. Our demonstrations imply a potential to construct a robust evolution system against constraint violations even in highly dynamical situations.

PACS numbers: 04.20.-q, 04.25.Dm, 04.25.-g

## I. INTRODUCTION

Numerical integration of the Einstein equations is the only way to investigate highly dynamical and nonlinear gravitational space-time. The detection of gravitational wave requires templates of waveform, among them mergers of compact objects are the most plausible astrophysical sources. Numerical relativity has been developed with this purpose over decades.

For neutron star (NS) binaries, a number of scientific numerical simulations have been done so far, and we are now at the level of discussing the actual physics of the phenomena, including the effects of the equations of state, hydrodynamics, and general relativity by evolving various initial data [1, 2, 3, 4, 5]. Mergers of black holes (BHs) are also available after the breakthrough by Pretorius [6] in 2004. Pretorius's implementation had many novel features in his code; among them he discretizes the four-dimensional Einstein equations directly, which is not a conventional approach so far. However, after the announcements of successful binary BH mergers by Campanelli et al. [7] and Baker et al. [8] based on the standard 3+1 decomposition of the Einstein equations, many groups began producing interesting results [9, 10, 11, 12, 13, 14, 15, 16, 17, 18]. The merger of NS-BH binary simulations has also been reported recently, e.g. [19].

Almost all the groups which apply the above conventional approach use the so-called BSSN variables together with “1 + log”-type slicing conditions for the lapse function and “ $\Gamma$ -driver” type slicing conditions for the shift

function. BSSN stands for Baumgarte-Shapiro [20] and Shibata-Nakamura [21], the modified Arnowitt-Deser-Misner formulation initially proposed by Nakamura [22]. (The details are described in §II A.) There have already been several efforts to explain why the combination of this recipe works from the point of view of the well-posedness of the partial differential equations (e.g. [23, 24]). However, the question remains whether there exists an alternative evolution system that enables more long-term stable and accurate simulations. The search for a better set of equations for numerical integrations is called the formulation problem for numerical relativity, of which earlier stages are reviewed by one of the authors [25].

In this article, we report our numerical tests of modified versions of the BSSN system, the *adjusted BSSN systems*, proposed by Yoneda and Shinkai [26]. The idea of their modifications is to add constraints to the evolution equations like Lagrange multipliers and to construct a robust evolution system which evolves to the constraint surface as the attractor. Their proposals are based on the eigenvalue analysis of the constraint propagation equations (the evolution equations of the constraints) on the perturbed metric. For the ADM formulation, they explain why the standard ADM does not work for long-term simulations by showing the existence of the constraint violating mode in perturbed Schwarzschild space-time [27]. For the BSSN formulation, they analyzed the eigenvalues of the constraint propagation equations only on flat space-time [26], but one of their proposed adjustments was immediately tested by Yo et al. [28] for the numerical evolution of Kerr-Schild space-time and confirmed to work as expected. (The details are described in §II B.)

Our numerical examples are taken from the proposed problems for testing the formulations of the Mexico Numerical Relativity Workshop 2001 participants [29],

---

\*kiuchi@gravity.phys.waseda.ac.jp

†shinkai@is.oit.ac.jp

which are sometimes called the Apples-with-Apples test. To concentrate the comparisons on the formulation problem, the templated problems are settled so as not to require technical complications; e.g., periodic boundary conditions are used and the slicing conditions do not require solving elliptical equations. Several groups already reported their code tests using these Apples tests (e.g. [30, 31, 32]), and we are also able to compare our results with theirs.

This article is organized as follows. We describe the BSSN equations and the *adjusted* BSSN equations in Sec. II A and II B. We give our three numerical test problems in Sec. III. Comments on our coding stuff are in Sec. IV. Sec. V is devoted to showing numerical results for each testbeds, and we summarize the results in Sec. VI.

## II. BASIC EQUATIONS

### A. BSSN equations

We start by presenting the standard BSSN formulation, where we follow the notations of [20], which are

widely used among numerical relativists.

The idea of the BSSN formulation is to introduce auxiliary variables to those of the Arnowitt-Deser-Misner (ADM) formulation for obtaining longer stable numerical simulations. The basic variables of the BSSN formulation are  $(\phi, \tilde{\gamma}_{ij}, K, \tilde{A}_{ij}, \tilde{\Gamma}^i)$ , which are defined by

$$\phi = \frac{1}{12} \log(\det \gamma_{ij}), \quad (2.1)$$

$$\tilde{\gamma}_{ij} = e^{-4\phi} \gamma_{ij}, \quad (2.2)$$

$$K = \gamma^{ij} K_{ij}, \quad (2.3)$$

$$\tilde{A}_{ij} = e^{-4\phi} \left[ K_{ij} - \frac{1}{3} \gamma_{ij} K \right], \quad (2.4)$$

$$\tilde{\Gamma}^i = \tilde{\gamma}^{jk} \tilde{\Gamma}_{jk}^i, \quad (2.5)$$

where  $(\gamma_{ij}, K_{ij})$  are the intrinsic and extrinsic ADM 3-metric. The conformal factor  $\phi$  is introduced so as to set  $\tilde{\gamma} \equiv \det[\tilde{\gamma}_{ij}]$  as unity,  $\tilde{A}_{ij}$  is supposed to be traceless, and  $\tilde{\Gamma}^i$  is treated independently in evolution equations. Therefore these three requirements turn into the new constraints [below (2.16)-(2.18)].

The set of the BSSN evolution equations are

$$\partial_t \phi = -\frac{1}{6} \alpha K + \beta^i \partial_i \phi + \frac{1}{6} \partial_i \beta^i, \quad (2.6)$$

$$\partial_t \tilde{\gamma}_{ij} = -2\alpha \tilde{A}_{ij} + \tilde{\gamma}_{ik} \partial_j \beta^k + \tilde{\gamma}_{jk} \partial_i \beta^k - \frac{2}{3} \tilde{\gamma}_{ij} \partial_k \beta^k + \beta^k \partial_k \tilde{\gamma}_{ij}, \quad (2.7)$$

$$\partial_t K = -D^i D_i \alpha + \alpha \tilde{A}_{ij} \tilde{A}^{ij} + \frac{1}{3} \alpha K^2 + \beta^i \partial_i K, \quad (2.8)$$

$$\begin{aligned} \partial_t \tilde{A}_{ij} = & -e^{-4\phi} [D_i D_j \alpha + \alpha R_{ij}]^{\text{TF}} + \alpha K \tilde{A}_{ij} - 2\alpha \tilde{A}_{ik} \tilde{A}^k_j \\ & + \partial_i \beta^k \tilde{A}_{kj} + \partial_j \beta^k \tilde{A}_{ki} - \frac{2}{3} \partial_k \beta^k \tilde{A}_{ij} + \beta^k \partial_k \tilde{A}_{ij}, \end{aligned} \quad (2.9)$$

$$\begin{aligned} \partial_t \tilde{\Gamma}^i = & -2\partial_j \alpha \tilde{A}^{ij} + 2\alpha \left[ \tilde{\Gamma}_{jk}^i \tilde{A}^{jk} - \frac{2}{3} \tilde{\gamma}^{ij} \partial_j K + 6\tilde{A}^{ij} \partial_j \phi \right] \\ & + \tilde{\gamma}^{jk} \partial_j \partial_k \beta^i + \frac{1}{3} \tilde{\gamma}^{ij} \partial_j \partial_k \beta^k + \beta^j \partial_j \tilde{\Gamma}^i - \tilde{\Gamma}^j \partial_j \beta^i + \frac{2}{3} \tilde{\Gamma}^i \partial_j \beta^j, \end{aligned} \quad (2.10)$$

where  $D_i$  is the covariant derivative with respect to the 3-metric  $\gamma_{ij}$  and TF means trace-free operation, i.e.,  $H_{ij}^{\text{TF}} = H_{ij} - \frac{1}{3} \gamma_{ij} H^k_k$ . The Ricci tensor is computed with the conformal connection  $\tilde{\Gamma}^i$  as

$$R_{ij} = R_{ij}^\phi + \tilde{R}_{ij}, \quad (2.11)$$

$$R_{ij}^\phi = -2\tilde{D}_i \tilde{D}_j \phi - 2\tilde{\gamma}_{ij} \tilde{D}^k \tilde{D}_k \phi + 4\tilde{D}_i \phi \tilde{D}_j \phi - 4\tilde{\gamma}_{ij} \tilde{D}^k \phi \tilde{D}_k \phi \quad (2.12)$$

$$\tilde{R}_{ij} = -\frac{1}{2} \tilde{\gamma}^{lk} \partial_k \partial_l \tilde{\gamma}_{ij} + \tilde{\gamma}_{k(i} \partial_{j)} \tilde{\Gamma}^k + \tilde{\gamma}^{lm} \tilde{\Gamma}_{lm}^k \tilde{\Gamma}_{(ij)k} + 2\tilde{\gamma}^{lm} \tilde{\Gamma}_{l(i} \tilde{\Gamma}_{j)km} + \tilde{\gamma}^{lm} \tilde{\Gamma}_{im}^k \tilde{\Gamma}_{klj}, \quad (2.13)$$

where  $\tilde{D}_i$  is a covariant derivative associated with  $\tilde{\gamma}_{ij}$ .

Similarly to the ADM formulation, this system has constraint equations. The two ‘‘kinematic’’ constraints,

the Hamiltonian and momentum constraint equations, are expressed in terms of the BSSN basic variables and are written as

$$\mathcal{H} = e^{-4\phi}\tilde{R} - 8e^{-4\phi}(\tilde{D}^i\tilde{D}_i\phi + \tilde{D}^i\phi\tilde{D}_i\phi) + \frac{2}{3}K^2 - \tilde{A}_{ij}\tilde{A}^{ij} - \frac{2}{3}\mathcal{A}K \approx 0, \quad (2.14)$$

$$\mathcal{M}_i = 6\tilde{A}^j{}_i\tilde{D}_j\phi - 2\mathcal{A}\tilde{D}_i\phi - \frac{2}{3}\tilde{D}_iK + \tilde{D}_j\tilde{A}^j{}_i \approx 0. \quad (2.15)$$

Additionally, the BSSN formulation requires three ‘‘algebraic’’ constraint relations;

$$\mathcal{G}^i = \tilde{\Gamma}^i - \tilde{\gamma}^{jk}\tilde{\Gamma}_{jk} \approx 0, \quad (2.16)$$

$$\mathcal{A} = \tilde{A}_{ij}\tilde{\gamma}^{ij} \approx 0, \quad (2.17)$$

$$\mathcal{S} = \tilde{\gamma} - 1 \approx 0, \quad (2.18)$$

where (2.16) and (2.17) are from the definitions of (2.5) and (2.4), respectively. Equation (2.18) is from the requirement on  $\tilde{\gamma}$ .

These five constraints are, theoretically, supposed to be zero at all times; therefore they can be used to modify the dynamical equations. For example, Alcubierre et al. [34] announced that the replacement of the terms in (2.10) using the momentum constraint drastically changes the stability feature. Actually, such replacements of terms using constraints are applied (with/without intentions) in many terms in (2.6)-(2.10), which are expressed as Eqs. (2.27)-(2.31) in [26].

Alcubierre et al. [35] also pointed out that the redefinition of  $\tilde{A}_{ij}$  by

$$\tilde{A}_{ij} \rightarrow \tilde{A}_{ij} - \frac{1}{3}\tilde{\gamma}_{ij}\text{tr}\tilde{A} \quad (2.19)$$

during the time evolutions improves the numerical stability. This technique again can be understood as the trace-out of the  $\mathcal{A}$ -constraint (2.17) from the evolution equations. In our numerical code, we do not apply this technique because we recognize the trace-free property as the new constraint  $\mathcal{A}$  in the BSSN system, and our purpose is to construct a system preventing the violation of constraints.

Recently, several groups applied artificial dissipation (e.g. [36]) to obtain stable evolutions (see, e.g. [32, 33, 37]). We, however, do not introduce such dissipations in our code, since we try to clarify the difference of stability from the viewpoint of *formulations* of the Einstein equations.

## B. Adjusted BSSN systems

To understand the stability property of the BSSN system, Yoneda and Shinkai [26] studied the structure of the evolution equations, (2.6)-(2.10), in detail, especially how the modifications using the constraints, (2.14)-(2.18), affect to the stability. They investigated the signature of the eigenvalues of the constraint propagation equations (dynamical equations of constraints), and explained that

the standard BSSN dynamical equations are balanced from the viewpoints of constrained propagations, including a clarification of the effect of the replacement using the momentum constraint equation.

Moreover, they predicted that several combinations of modifications have a constraint-damping nature, and named them *adjusted* BSSN systems. (Their predictions are based on the signature of eigenvalues of the constraint propagations, and the negative signature implies a dynamical system which evolves toward the constraint surface as the attractor.)

Among them, in this work, we test the following three adjustments:

1. An adjustment of the  $\tilde{A}$ -equation with the momentum constraint:

$$\partial_t\tilde{A}_{ij} = \partial_t^B\tilde{A}_{ij} + \kappa_A\alpha\tilde{D}_{(i}\mathcal{M}_{j)}, \quad (2.20)$$

where  $\kappa_A$  is predicted (from the eigenvalue analysis) to be positive in order to damp the constraint violations.

2. An adjustment of the  $\tilde{\gamma}$ -equation with  $\mathcal{G}$  constraint:

$$\partial_t\tilde{\gamma}_{ij} = \partial_t^B\tilde{\gamma}_{ij} + \kappa_{\tilde{\gamma}}\alpha\tilde{\gamma}_{k(i}\tilde{D}_{j)}\mathcal{G}^k, \quad (2.21)$$

with  $\kappa_{\tilde{\gamma}} < 0$ .

3. An adjustment of the  $\tilde{\Gamma}$ -equation with  $\mathcal{G}$  constraint:

$$\partial_t\tilde{\Gamma}^i = \partial_t^B\tilde{\Gamma}^i + \kappa_{\tilde{\Gamma}}\alpha\mathcal{G}^i. \quad (2.22)$$

with  $\kappa_{\tilde{\Gamma}} < 0$ .

These three adjustments are chosen as samples of ‘‘best candidates’’, Eq. (4.9)-(4.11) in [26]. The term ‘‘best’’ comes from their conjecture on the eigenvalue analysis of the constraint propagation matrix; that is, (a) all the resultant eigenvalues from above adjustments can be less than or at most equal to zero, which indicates the decay of constraint errors, and (b) the resultant constraint propagation matrix is diagonalizable, which guarantees the predictions of above eigenvalue analysis (see Table II in [26]). However, since above eigenvalues include zero elements and also above analysis assumes a linearly perturbed metric about the flat space-time, the effects of the adjustments (2.20)-(2.22) need to be demonstrated via numerical experiments.

### III. NUMERICAL TESTBED MODELS

Following the proposals of the Mexico Numerical Relativity Workshop [29], we perform three kinds of tests. In this section, we explicitly give some details of the models.

#### A. Gauge-wave testbed

The first test is the trivial Minkowski space-time, but sliced with the time-dependent 3-metric, which is called the gauge-wave test. The 4-metric is obtained by coordinate transformation from the Minkowski metric as

$$ds^2 = -Hdt^2 + Hdx^2 + dy^2 + dz^2, \quad (3.1)$$

where

$$H = H(x-t) = 1 - A \sin\left(\frac{2\pi(x-t)}{d}\right), \quad (3.2)$$

which describes a sinusoidal gauge wave of amplitude  $A$  propagating along the  $x$ -axis. The non-trivial extrinsic curvature is

$$K_{xx} = -\frac{\pi A}{d} \frac{\cos\left(\frac{2\pi(x-t)}{d}\right)}{\sqrt{1 + A \sin\frac{2\pi(x-t)}{d}}}. \quad (3.3)$$

Following [29], we chose numerical domain and parameters as follows:

- Gauge-wave parameters:  $d = 1$  and  $A = 10^{-2}$
- Simulation domain:  $x \in [-0.5, 0.5]$ ,  $y = z = 0$
- Grid:  $x^i = -0.5 + (n - \frac{1}{2})dx$  with  $n = 1, \dots, 50\rho$ , where  $dx = 1/(50\rho)$  with  $\rho = 2, 4, 8$
- Time step:  $dt = 0.25dx$
- Boundary conditions: Periodic boundary condition in  $x$  direction and planar symmetry in  $y$  and  $z$  directions
- Gauge conditions:

$$\partial_t \alpha = -\alpha^2 K, \quad \beta^i = 0. \quad (3.4)$$

The 1D simulation is carried out for a  $T = 1000$  crossing-time or until the code crashes, where one crossing-time is defined by the length of the simulation domain.

#### B. Linear wave testbed

The second test is to check the ability of handling a travelling gravitational wave. The initial 3-metric and extrinsic curvature  $K_{ij}$  are given by a diagonal perturbation with component

$$ds^2 = -dt^2 + dx^2 + (1+b)dy^2 + (1-b)dz^2, \quad (3.5)$$

where

$$b = A \sin\left(\frac{2\pi(x-t)}{d}\right) \quad (3.6)$$

for a linearized plane wave traveling in the  $x$ -direction. Here  $d$  is the linear size of the propagation domain and  $A$  is the amplitude of the wave. The non-trivial components of extrinsic curvature are then

$$K_{yy} = -\frac{1}{2}\partial_t b, \quad K_{zz} = \frac{1}{2}\partial_t b. \quad (3.7)$$

Following [29], we chose the following parameters:

- Linear wave parameters:  $d = 1$  and  $A = 10^{-8}$
- Simulation domain:  $x \in [-0.5, 0.5]$ ,  $y = 0$ ,  $z = 0$
- Grid:  $x^i = -0.5 + (n - \frac{1}{2})dx$  with  $n = 1, \dots, 50\rho$ , where  $dx = 1/(50\rho)$  with  $\rho = 2, 4, 8$
- Time step:  $dt = 0.25dx$
- Boundary conditions: Periodic boundary condition in  $x$  direction and planar symmetry in  $y$  and  $z$  directions
- Gauge conditions:  $\alpha = 1$  and  $\beta^i = 0$

The 1D simulation is carried out for a  $T = 1000$  crossing-time or until the code crashes.

#### C. Collapsing polarized Gowdy-wave testbed

The third test is to check the formulation in a strong field context using the polarized Gowdy metric, which is written as

$$ds^2 = t^{-1/2}e^{\lambda/2}(-dt^2 + dz^2) + t(e^P dx^2 + e^{-P} dy^2) \quad (3.8)$$

Here time coordinate  $t$  is chosen such that time increases as the universe expands. Simple forms of the solutions,  $P$  and  $\lambda$ , are given by

$$\begin{aligned} P &= J_0(2\pi t) \cos(2\pi z), \\ \lambda &= -2\pi t J_0(2\pi t) J_1(2\pi t) \cos^2(2\pi z) \\ &\quad + 2\pi^2 t^2 [J_0^2(2\pi t) + J_1^2(2\pi t)] \\ &\quad - \frac{1}{2} [(2\pi)^2 [J_0^2(2\pi) + J_1^2(2\pi)] \\ &\quad - 2\pi J_0(2\pi) J_1(2\pi)], \end{aligned} \quad (3.10)$$

where  $J_n$  is the Bessel function. The non-trivial extrinsic curvatures are then

$$K_{xx} = -\frac{1}{2} t^{1/4} e^{-\lambda/4} e^P (1 + tP_{,t}), \quad (3.11)$$

$$K_{yy} = -\frac{1}{2} t^{1/4} e^{-\lambda/4} e^{-P} (1 - tP_{,t}), \quad (3.12)$$

$$K_{zz} = \frac{1}{4} t^{-1/4} e^{\lambda/4} (t^{-1} - \lambda_{,t}). \quad (3.13)$$

According to [29], the new time coordinate  $\tau$ , which satisfies harmonic condition, is obtained by coordinate transformation as

$$t(\tau) = ke^{c\tau}, \quad (3.14)$$

where  $c$  and  $k$  are arbitrary constants. Using this freedom, we can set the lapse function in the new time coordinate to be unity at the initial time. Concretely, we set

$$\begin{aligned} t_0 = \tau_0 &\sim 9.8753205829098, \\ c &\sim 0.0021195119214617, \\ k &\sim 9.6707698127638, \end{aligned} \quad (3.15)$$

where  $t_0$  is the initial time. Following [29], we perform our evolution in the collapsing (i.e. backward in time) direction. Parameters are chosen as follows:

- Simulation domain:  $z \in [-0.5, 0.5]$ ,  $x = y = 0$
- Grid:  $z = -0.5 + (n - \frac{1}{2})dz$  with  $n = 1, \dots, 50\rho$ , where  $dz = 1/(50\rho)$  with  $\rho = 2, 4, 8$
- Time step:  $dt = 0.25dz$
- Boundary conditions: Periodic boundary condition in  $z$ -direction and plane symmetry in  $x$ - and  $y$ -directions
- Gauge conditions: the harmonic slicing (3.4) and  $\beta^i = 0$

The 1D simulation is carried out for a  $T = 1000$  crossing-time or until the code crashes.

## IV. THE CODE

### A. Code description

We have developed a new numerical code based on the adjusted BSSN systems. The variables are  $(\phi, \tilde{\gamma}_{ij}, K, A_{ij}, \tilde{\Gamma}^i)$ , and the evolution equations are (2.6)-(2.10) with/without adjustment (2.20), (2.21), and/or (2.22). The time-integration is under the free-evolution scheme, and we monitor five constraints, (2.14)-(2.18), to check the accuracy and stability of the evolutions.

Our time-integration scheme is the three-step iterative Crank-Nicholson method with centered finite difference in space [39]. This scheme should have second-order convergence both in space and time, and we checked its convergence in all the testbeds.

As we have already mentioned in the end of §II A, we do not apply the trace-out technique of  $\tilde{A}_{ij}$ , (2.19) in our code.

We also remark on our treatment of the conformal connection variable  $\tilde{\Gamma}^i$ . As was pointed out in [38], it is better not to use  $\tilde{\Gamma}^i$  in all the evolution equations. We surmise this is because the amplification of the error due to the

discrepancy of the definition (2.5), i.e., the accumulations of the violations of  $\mathcal{G}^i$ -constraint (2.16). Therefore, we used the evolved  $\tilde{\Gamma}^i$  only for the terms in (2.10) and (2.13), and not for other terms, so as not to implicitly apply the  $\mathcal{G}^i$ -constraint in time evolutions.

### B. Debugging procedures

It is crucial that our code can produce accurate results, because the adjustment methods are based on the assumption that the code represents the BSSN system (2.6)-(2.10) accurately. We verified our code by comparing our numerical data with analytic solutions from the gauge-wave and Gowdy-wave testbeds in Sec. III. The actual procedures are as follows:

1. Evolve only one component, e.g.  $\tilde{A}_{xx}$ , numerically, and express all the other components with those of the analytic solution. In this situation, the origin of the error is from the finite differencing of the analytic solution in the spatial direction and from that of the numerically evolved component ( $\tilde{A}_{xx}$ ) both in spatial and time directions. We checked the code by monitoring the difference between the numerically evolved component ( $\tilde{A}_{xx}$ ) and its analytic expression. This procedure was applied to all the components one by one.
2. Evolve only several components, e.g.,  $\tilde{A}_{xx}$  and  $\tilde{\Gamma}^x$ , numerically, and express the other components by the analytic solution. The error can be checked by a procedure similar to the one above.
3. Evolve all the components numerically, and check the error with the analytic solution.

We repeated these procedure three times by switching the propagation directions ( $x$ ,  $y$ , and  $z$ -directions) of gauge-wave and Gowdy-wave solutions. We also applied these procedures in a 2D test [29], and checked the off-diagonal component.

### C. Error evaluation methods

It should be emphasized that the adjustment effect has two meanings, improvement of stability and of accuracy. Even if a simulation is stable, it does not imply that the result is accurate. We judge the stability of the evolution by monitoring the L2 norm of each constraint,

$$\|\delta\mathcal{C}\|_2(t) \equiv \sqrt{\frac{1}{N} \sum_{x,y,z} (\mathcal{C}(t; x, y, z))^2}, \quad (4.1)$$

where  $N$  is the total number of grid points, while we judge the accuracy by the difference of the metric components  $g_{ij}(t; x, y, z)$  from the exact solution

$$g_{ij}^{(\text{exact})}(t; x, y, z),$$

$$\|\delta g_{ij}\|_2(t) \equiv \sqrt{\frac{1}{N} \sum_{x,y,z} \left( g_{ij} - g_{ij}^{(\text{exact})} \right)^2}. \quad (4.2)$$

#### D. Magnitude of $\kappa$

Adjusted systems, (2.20)-(2.22), require to specify the parameter  $\kappa$ . From the analytical prediction in [26] we know the signature of  $\kappa$ , but not for its magnitude. By definition of the adjustment terms in Eq. (2.20)-(2.22), applying small  $\kappa$  should produce the close results with those of the plain system. On the contrary, the large  $\kappa$  system will violate the Courant-Friedrich-Lewy condition [40]. Hence, there exists a suitable region in the adjustment parameters.

At this moment, we have to chose  $\kappa$  experimentally, by observing the life-time of simulations. The value of  $\kappa$ , used in our demonstrations, is one of the choices of which the adjustment works effectively in all the resolutions.

### V. NUMERICAL RESULTS

#### A. Gauge-wave test

##### 1. The plain BSSN system

As the first test, we show the plain BSSN evolution (that is, no adjustments) in Fig. 1 for the gauge-wave test. In Fig. 1, the L2 norms of the Hamiltonian and momentum constraints (4.1) are plotted as a function of the crossing-time. The second-order convergent nature is lost at an early time, the 20 crossing-time, and the simulation crashes at about the 100 crossing-time. The poor performance of the plain BSSN system for the gauge wave test has been reported in [31] (see their Fig. 8). This drawback, on the other hand, can be overcome if one uses the fourth-order finite differencing scheme, an example of which can be seen in [32] (see their Fig. 2).

##### 2. Adjusted BSSN with $\tilde{A}$ -equation

We found that the simulation lasts 10 times longer with the adjustment in the  $\tilde{A}$ -equation using the momentum constraint (2.20). Figure 2 shows the L2 norms of the Hamiltonian and Momentum constraints in the same style as in Fig. 1. The adjustment parameter is set at  $\kappa_A = 0.005$  for this plot. We obtain almost perfect overlap of the rescaled Hamiltonian constraint for 200 crossing-times and almost perfect overlap in the momentum constraint for 50 crossing-times; there apparently improve the results of the plain BSSN system (see Fig. 1). We show the plots until the 1000 crossing-time, there we observe the growth of the error both in later time and in

higher resolution cases. However, it is also true that all errors are still under the errors of the plain BSSN system. Therefore, we conclude that this adjusted system shows a weaker instability than the plain system.

##### 3. Adjusted BSSN with $\tilde{\Gamma}$ -equation

The case of the adjustment of the  $\tilde{\Gamma}$ -equation using the  $\mathcal{G}$  constraint (2.22) is shown in Fig. 3.

The adjustment parameter is set at  $\kappa_{\tilde{\Gamma}} = -0.1$ . We find that the second-order convergence breaks down near the 40 crossing-time under the Momentum constraint, which is almost the same as with the plain BSSN system. However, the convergence of the Hamiltonian constraint is improved, i.e., it continues to the near 55 crossing-time. The life-time of the simulation is almost the same as that of the plain BSSN system.

##### 4. Adjusted BSSN with $\tilde{\gamma}$ -equation

We also tested the cases of the adjustment of the  $\tilde{\gamma}$ -equation using the  $\mathcal{G}$  constraint, (2.21). We again observed the effects of the adjustment on its stability and accuracy but found a rather small effect compared to the cases of the adjustments of (2.20) or (2.22), up to our trials of the parameter range of  $\kappa_{\tilde{\gamma}}$ . Therefore we omit showing the results.

##### 5. Evaluation of Accuracy

For evaluating the accuracy, we prepare Fig. 4(a), in which we plot the L2 norm of the error in  $\gamma_{xx}$ , (4.2), with the function of time. Three lines correspond to the result of the plain BSSN system,  $\tilde{A}$ -eq. adjusted, and  $\tilde{\Gamma}$ -eq. adjusted BSSN system, respectively. The  $\tilde{\Gamma}$ -adjustment makes the life-time slightly longer than that of the plain BSSN, while  $\tilde{A}$ -adjustment increases the life-time of the simulation by a factor of 10. However, it is also true that the error grows in time in all the three cases.

We also find that the error is induced by distortion of the wave, i.e. the both phase and amplitude errors distort the numerical solution. In Fig. 4(b), we show a snapshot of  $\gamma_{xx}$  numerical solution at  $T = 100$ , together with the exact solution at the same time coordinate. The amplitude difference between the numerical and exact solutions is apparently less when we use the  $\tilde{A}$ -eq. adjusted system than that of the plain system. In Sec. VI later, we discuss what causes the error and why the simulation life-time becomes longer when we use the adjusted system.

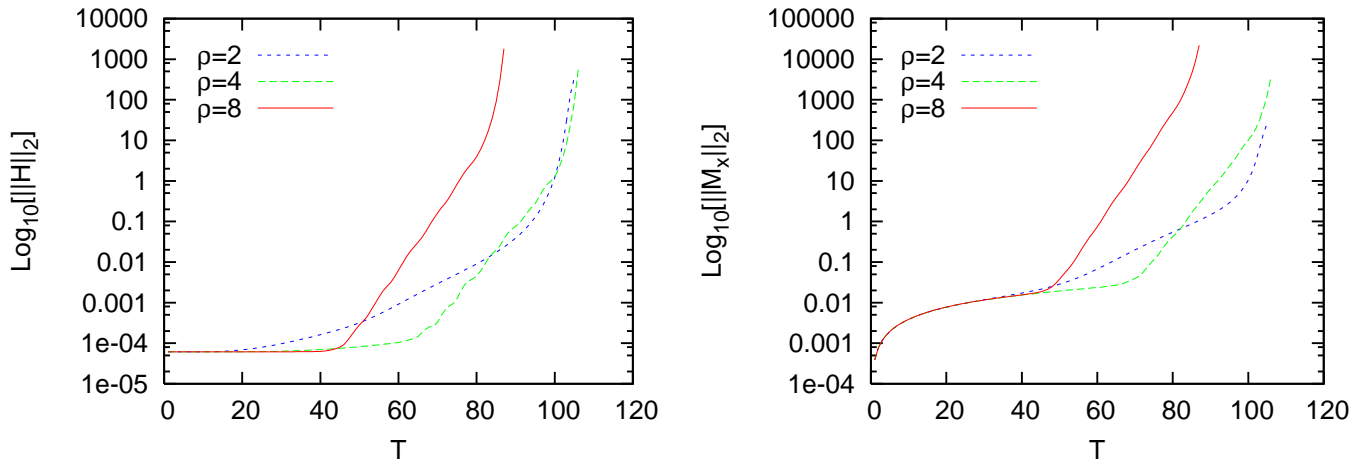


FIG. 1: The one-dimensional gauge-wave test with the plain BSSN system. The L2 norm of  $\mathcal{H}$  and  $\mathcal{M}_x$ , rescaled by  $\rho^2/4$ , are plotted with a function of the crossing-time. The amplitude of the wave is  $A = 0.01$ . The loss of convergence at the early time, near the 20 crossing-time, can be seen, and it will produce the blow-ups of the calculation in the end.

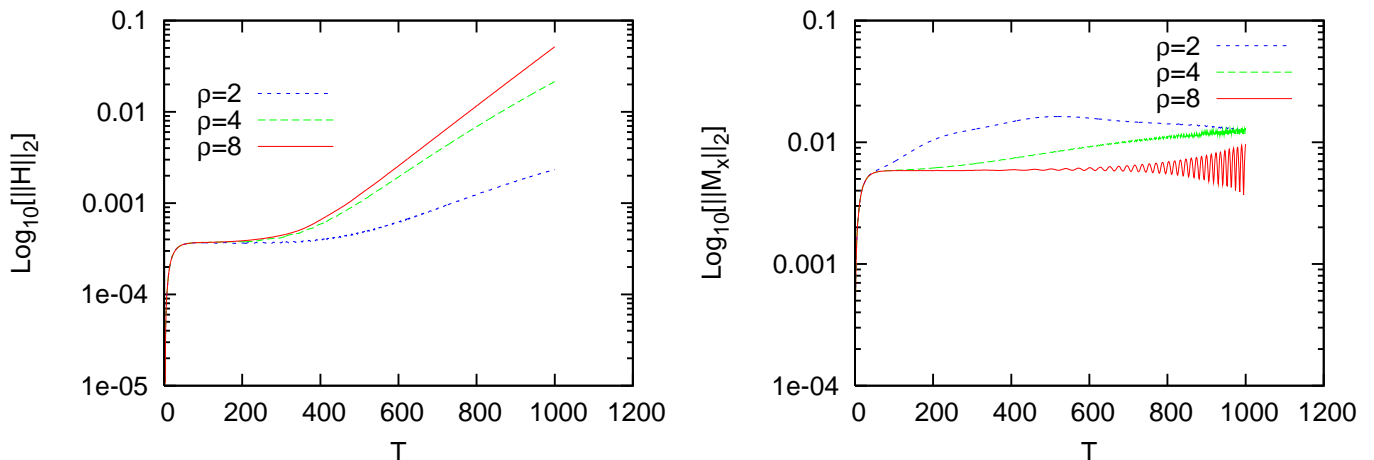


FIG. 2: The one-dimensional gauge-wave test with the adjusted BSSN system in the  $\tilde{A}$ -equation (2.20). The L2 norm of  $\mathcal{H}$  and  $\mathcal{M}_x$ , rescaled by  $\rho^2/4$ , are plotted with a function of the crossing-time. The wave parameter is the same as with Fig. 1, and the adjustment parameter  $\kappa_A$  is set to  $\kappa_A = 0.005$ . We see the higher resolution runs show convergence longer, i.e., the 300 crossing-time in  $\mathcal{H}$  and the 200 crossing-time in  $\mathcal{M}_x$  with  $\rho = 4$  and 8 runs. All runs can stably evolve up to the 1000 crossing-time.

### B. Linear wave test

The second test is the linear wave propagation test, §III B, to check the accuracy of wave propagations in the adjusted systems. We find that the linear wave testbed

does not produce a significant constraint violation even for the plain BSSN system. The simulation does not crash at the 1000 crossing-time irrespective of the resolutions. Figure 5 illustrates the profiles of  $\gamma_{zz} - 1$  at the 500 crossing-time. The figure indicates the simulation does not produce the amplitude error but does pro-

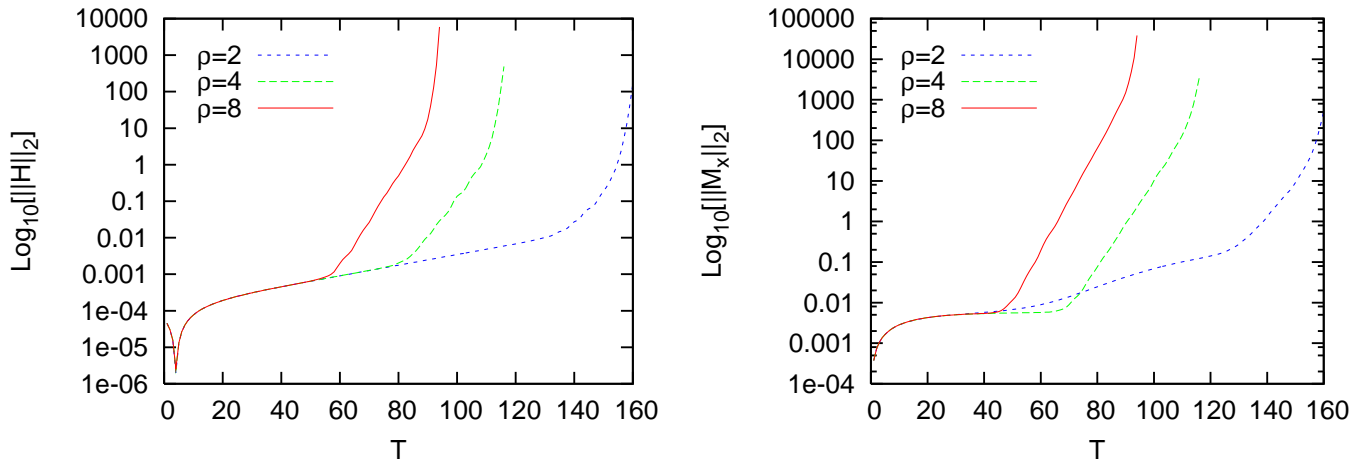


FIG. 3: The one-dimensional gauge-wave test with the adjusted BSSN system in the  $\tilde{\Gamma}$ -equation (2.22). The L2 norm of  $\mathcal{H}$  and  $\mathcal{M}_x$ , rescaled by  $\rho^2/4$ , are plotted with a function of the crossing-time. The wave parameter is the same as Fig. 1, and the adjustment parameter is  $\kappa_{\tilde{\Gamma}} = -0.1$ . Note the near perfect overlap for the 55 crossing-time in  $\mathcal{H}$  and the 40 crossing-time in  $\mathcal{M}_x$ .

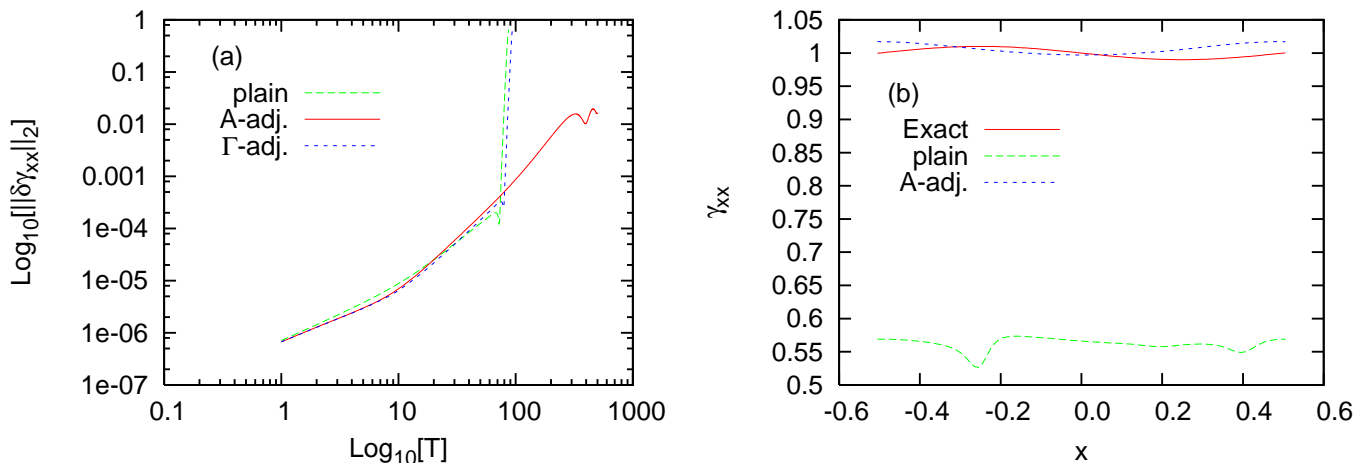


FIG. 4: Evaluation of the accuracy of the one-dimensional gauge-wave testbed. Lines show the plain BSSN, the adjusted BSSN with  $\mathcal{A}$ -equation, and with  $\tilde{\Gamma}$ -equation. (a) The L2 norm of the error in  $\gamma_{xx}$ , using (4.2). (b) A snapshot of the exact and numerical solution at  $T = 100$ .

duce the phase error. However, we also observe that the higher resolution run reduces the phase error. We tried the same evolutions with adjusted BSSN systems. However, all the results are indistinguishable from the those of the plain BSSN system. This is because the adjusted terms of the equations are small due to the small violations of constraints. Figure 6 shows a snapshot of the error defined by  $\gamma_{zz} - \gamma_{zz}^{(\text{exact})}$  at the 500 crossing-time both for the plain BSSN system and the adjusted BSSN system where the  $\tilde{A}$ -equation where  $\kappa_{\mathcal{A}} = 10^{-3}$ . Since

two lines are matching quite well, we can say that the adjusted BSSN system produces the same result as the plain BSSN system, including the phase error. Results from the other adjusted BSSN systems are almost the same qualitatively, including their convergence features. We also remark that we do not see a case in which adjustment worsens accuracy and stability.

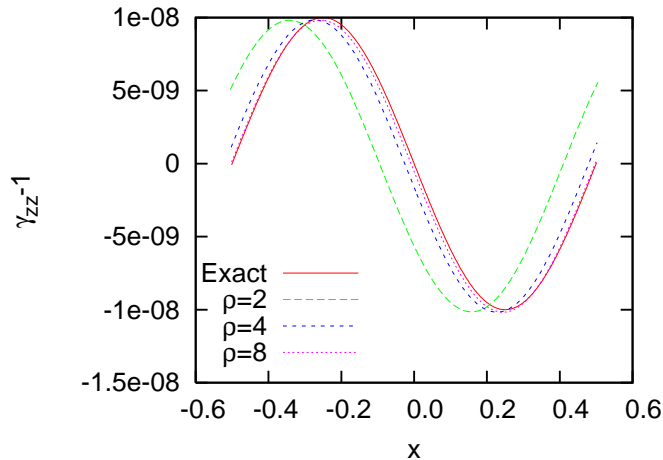


FIG. 5: Snapshots of the one-dimensional linear wave at different resolutions with the plain BSSN system at the simulation time 500 crossing-time. We see there exists phase error, but they are convergent away at higher resolution runs.

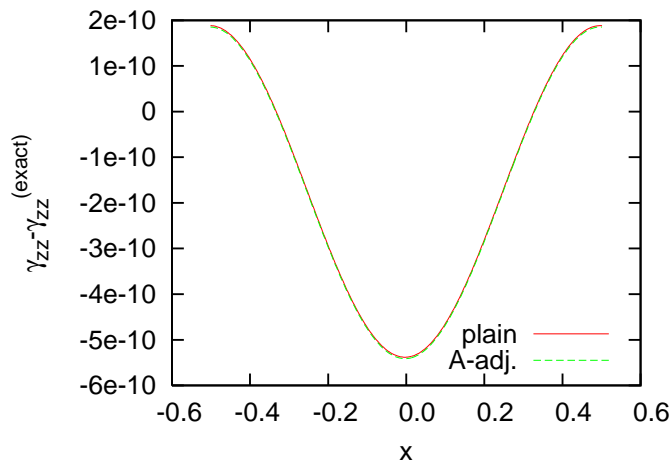


FIG. 6: Snapshot of errors with the exact solution for the Linear Wave testbed with the plain BSSN system and the adjusted BSSN system with the  $\tilde{A}$  equation at  $T = 500$ . The highest resolution  $\rho = 8$  is used in both runs. The difference between the plain and the adjusted BSSN system with the  $\tilde{A}$  equation is indistinguishable. Note that the maximum amplitude is set to be  $10^{-8}$  in this problem.

### C. Gowdy-wave test

The third test is the polarized Gowdy-wave test, §III C, to check the adjustments in the strong field regime.

#### 1. The plain BSSN

In Fig. 7, We first show the case of the plain BSSN evolution. We find that the second-order convergence continues up-to the 100 crossing-time and the higher resolutions runs tend to crash at early times. This behavior (and crashing time) almost coincides with the results of the *Cactus* BSSN code, reported by Alcubierre et al. [29] (see their Fig. 7). (We remark that Zlochower et al. [32]

reported they can produce the stable and accurate evolution for the 1000 crossing-time by implementing the higher order differencing scheme to their *LazEv* code. However, it should be emphasized that they suggested their code produces the stable simulation only when they used the Kreiss-Oliger dissipation term [36].)

#### 2. Adjusted BSSN with $\tilde{A}$ -equation

Adjustment of the  $\tilde{A}$ -equation using the momentum constraint (2.20), extends the life-time of the simulation 10 times longer for the highest resolution run. Figure 8 depicts the rescaled L2 norm of  $\mathcal{H}$  and  $\mathcal{M}_z$  versus time. We set  $\kappa_{\mathcal{A}} = -0.001$ . (Note that the signature of  $\kappa$  is

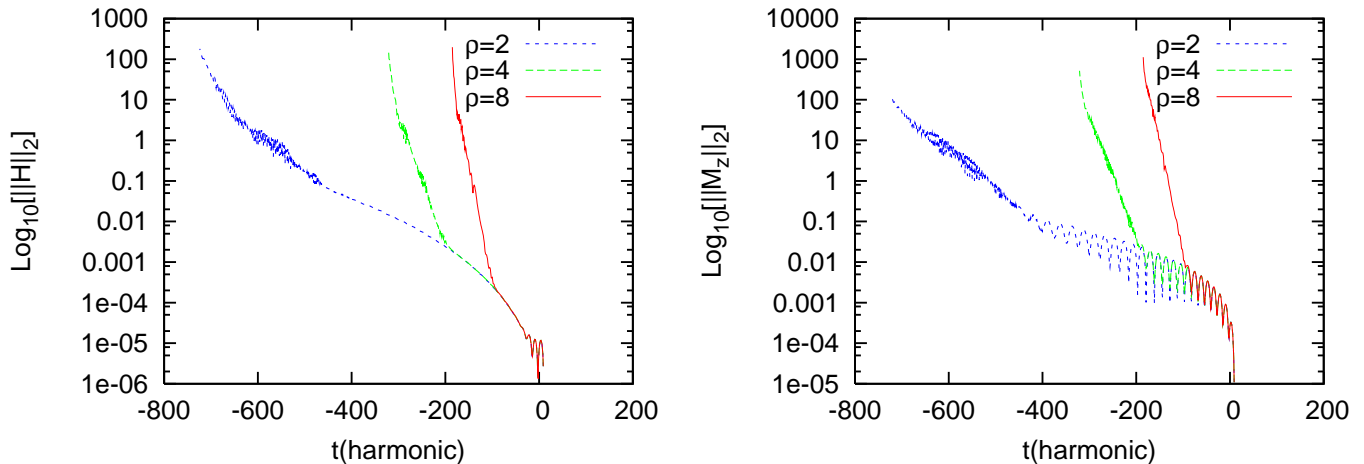


FIG. 7: Collapsing polarized Gowdy-wave test with the plain BSSN system. The L2 norm of  $\mathcal{H}$  and  $\mathcal{M}_z$ , rescaled by  $\rho^2/4$ , are plotted with a function of the crossing-time. (Simulation proceeds backwards from  $t = 0$ .) We see almost perfect overlap for the initial 100 crossing-time, and the higher resolution runs crash earlier. This result is quite similar to those achieved with the Cactus BSSN code, reported by [29].

reversed from the expected one, since the evolution is backward in time.)

We find that an almost perfect overlap up to the 1000 crossing-time under both the Hamiltonian constraint and the Momentum constraint. (These overlaps indicate that the error in  $\mathcal{H}$  and  $\mathcal{M}_z$  in the  $\rho = 8$  resolution runs are 16 times smaller than these errors in the  $\rho = 2$  resolution run. ) However, we also find oscillations in the Momentum constraint, especially in the end of the simulation.

### 3. Adjusted BSSN with $\tilde{\gamma}$ -equation

The case of the adjustment of the  $\tilde{\gamma}$ -equation using the  $\mathcal{G}$ -constraint (2.21), is shown in Fig. 9. The adjustment parameter  $\kappa_{\tilde{\gamma}}$  is set at 0.000025. (Again, the signature of  $\kappa$  is reversed from the expected one.)

Figure 9 shows that an almost perfect overlap is obtained for the 200 crossing-time in both  $\mathcal{H}$  and  $\mathcal{M}_z$ . The higher resolution runs tend to crash at earlier times, which is same as with the plain BSSN system. However, the convergence time becomes longer than that of the plain BSSN system. We will discuss the quantitative improvement for the  $\tilde{\gamma}$ -adjustment in the next subsection.

### 4. Adjustment effect

In order to check the *accuracy* of the simulations, we prepare Fig. 10 to show the error of the  $\gamma_{zz}$  component

of the metric.

Unlike the gauge-wave or the linear wave test, in this Gowdy-wave test the amplitude of the metric functions damps with time. Therefore we use the criterion that the error normalized by  $\gamma_{zz}$  be under 1% for an *accurate evolution*. This criterion is the same as the one used in Zlochower et al. [32].

Figure 10 shows the normalized error in  $\gamma_{zz}$  versus time for the plain BSSN, adjusted BSSN with  $\mathcal{A}$ -equation, and adjusted BSSN with  $\tilde{\gamma}$ -equation systems. We find that these three systems produce accurate results up to  $t = 200$ ,  $t = 1000$ , and  $t = 400$ , respectively. This proves that the adjustments work effectively, i.e, they make possible a stable and accurate simulation, especially the  $\mathcal{A}$ -adjusted BSSN system.

## VI. SUMMARY AND DISCUSSION

In this article, we presented our numerical comparisons of the BSSN formulation and its adjusted versions using constraints. We performed three testbeds: gauge-wave, linear wave, and collapsing polarized Gowdy-wave tests with their evolutions by three kinds of adjustments, which were previously proposed by Yoneda and Shinkai [26] based on their constraint propagation analysis.

The idea of the adjusted systems is to construct a system robust against constraint violations by modifying the evolution equations using the constraint equations.

We can summarize our tests as follows:

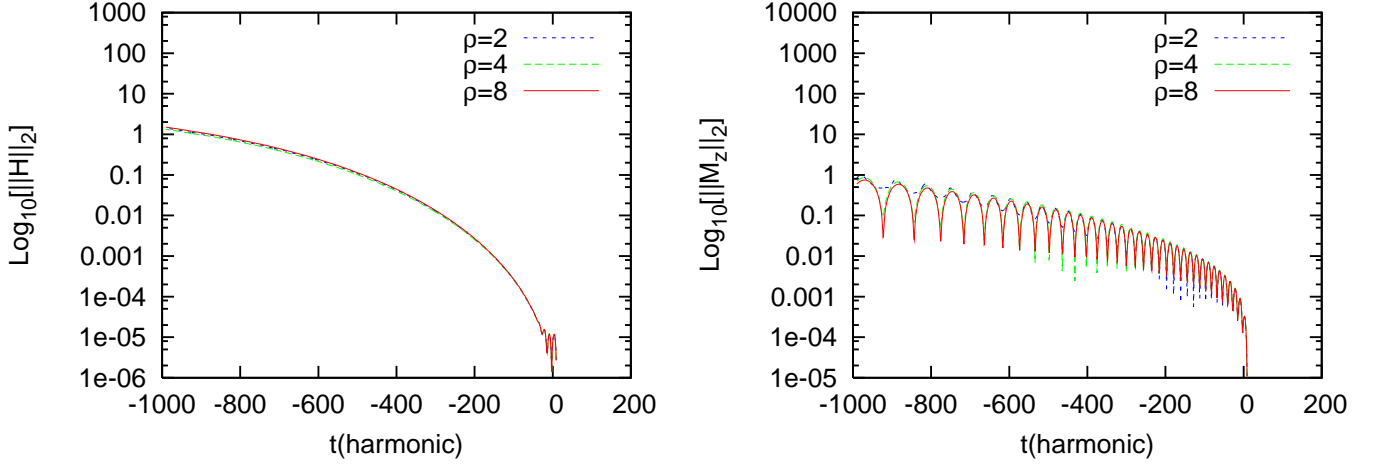


FIG. 8: Collapsing polarized Gowdy-wave test with the adjusted BSSN system in the  $\tilde{A}$ -equation (2.20), with  $\kappa_A = -0.001$ . The style is the same as in Fig. 7 and note that both constraints are normalized by  $\rho^2/4$ . We see almost perfect overlap for the initial 1000 crossing-time in both constraint equations,  $\mathcal{H}$  and  $\mathcal{M}_z$ , even for the highest resolution run.

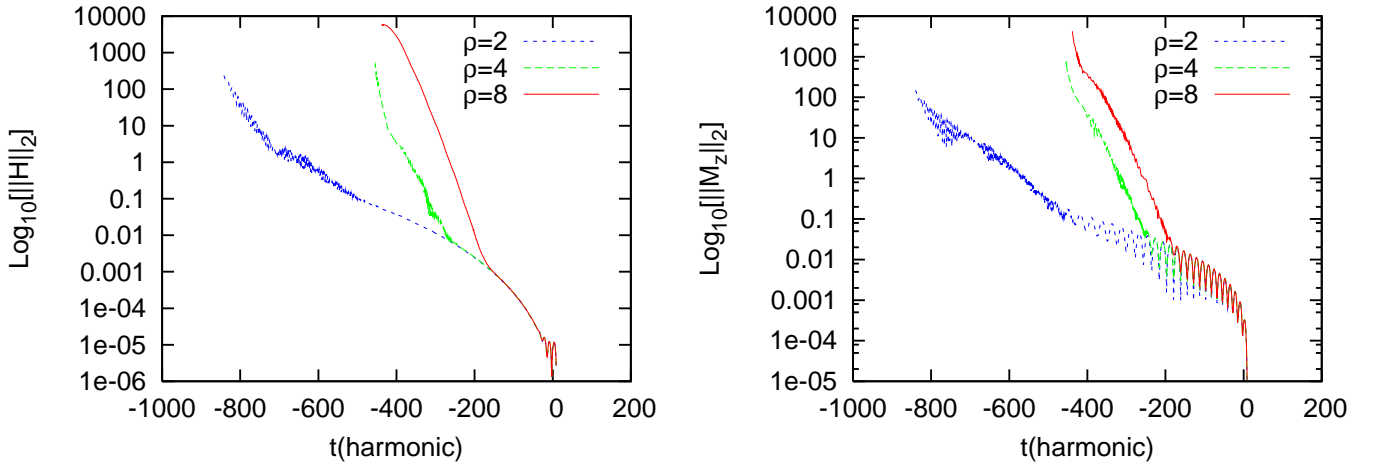


FIG. 9: Collapsing polarized Gowdy-wave test with the adjusted BSSN system in the  $\tilde{\gamma}$ -equation (2.21), with  $\kappa_{\tilde{\gamma}} = 0.000025$ . The figure style is the same as Figure 7. Note the almost perfect overlap for 200 crossing-time in the both the Hamiltonian and Momentum constraint and the  $\rho = 2$  run can evolve stably for 1000 crossing-time.

- When the plain (original) BSSN evolutions already show satisfactory good evolutions (e.g., the linear wave test), the constraint violations (i.e., adjusted terms) are also small or ignorable.

Therefore the adjusted BSSN equations become quite similar to the plain BSSN equations, and their results coincide with the plain BSSN results.

- Among the adjustments we tried, we observed that the adjusted BSSN system with the  $\tilde{A}$ -eq. (2.20) is the most robust for all the testbeds examined in this study. It gives us an accurate and stable evolution compared to the plain BSSN system. Quantitatively, the life-time of the simulation becomes 10 times longer for the gauge-wave testbed and 5 times longer for the Gowdy-wave testbed than the

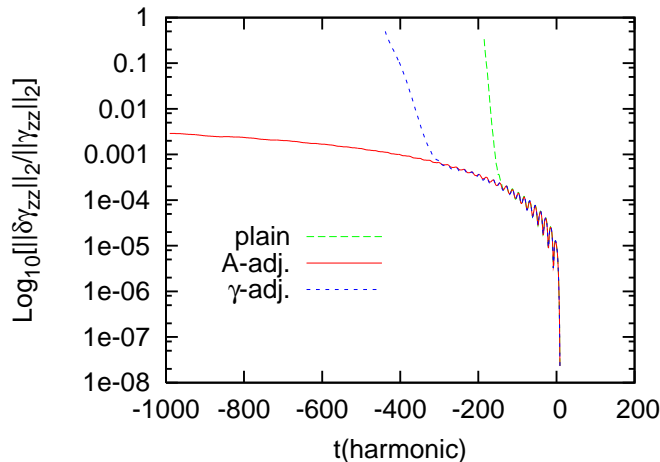


FIG. 10: Comparisons of systems in the collapsing polarized Gowdy-wave test. The L2 norm of the error in  $\gamma_{zz}$ , rescaled by the L2 norm of  $\gamma_{zz}$ , for the plain BSSN, adjusted BSSN with  $\tilde{A}$ -equation, and with  $\tilde{\gamma}$ -equation are shown. The highest resolution run,  $\rho = 8$ , is depicted for the plots. We can conclude that the adjustments make longer accurate runs available. Note that the evolution is backwards in time.

life-time of the plain BSSN system. However, it should be noted that for the gauge-wave testbed, the convergence feature is lost at a comparatively early time, the 200 crossing-time in the Hamiltonian constraint and the 50 crossing-time in the momentum constraint.

Recently, it has been claimed that the set up of the gauge wave problem in Apples-with-Apples has a problematic point [37], which arises from the harmonic gauge condition. In [41], it is argued that this gauge has a residual freedom in the form  $H \rightarrow e^{\lambda t} H$ , where  $\lambda$  is an arbitrary and  $H$  is a function in Eq. (3.1). Of course, our set up corresponds to the  $\lambda = 0$  case, but numerical error easily excites modes that result in either exponentially increasing or decaying metric amplitude. Actually, we find the amplitude of the error decays with time in this testbed. So, we conclude that due to the adjustment, the growing rate of the gauge mode is suppressed and the life-time of the simulation is extended as a result.

- The other type of adjustments (2.21 and 2.22) show their apparent effects while depending on a problem. The  $\tilde{\Gamma}$ -adjustment for the gauge-wave testbed makes the life-time longer slightly. The  $\tilde{\gamma}$ -adjustment for the Gowdy-wave testbed makes possible a simulation twice as long as the plain BSSN system.

We can understand the effect of the adjustments in terms of adding dissipative terms. By virtue of the definition of the constraints, we can recognize that the adjusted equation corresponds to the diffusion equation (see, for example, Eq. (2.20)) and the signature of  $\kappa$  determines whether the diffusion is positive or negative. In the adjusted  $\tilde{A}$ -eq. system, (2.20), the adjustment term corresponds to the positive diffusive term, due to the defini-

tion of  $\mathcal{M}_i$  and the positiveness of  $\kappa_A$  (see Eq. (2.15) and (2.20)). This fact might explain why the adjusted  $\tilde{A}$ -eq. system works effectively for all the testbeds.

In contrast, why are not all the adjustments effective in all testbeds? As we mentioned in Sec. IIB, the eigenvalue analysis was made on the linearly perturbed violation of constraints on the Minkowski space-time. Since the constraint violation grows non-linearly as seen in the Appendix of [26], the candidates may not be the best in their later evolution phase.

We remark upon two more interesting aspects arising from our study. The first is the mechanism of the constraint violations. As was shown in the appendix of [26], each constraint propagation (behavior of their growth or decrease) depends on the other constraint terms together with itself. That is, we can guess  $\mathcal{A}$  and  $\mathcal{S}$  constraints (2.17 and 2.18) in this article, propagate independently of the other constraints, while the violation of the  $\mathcal{G}$ -constraint, (2.16) is triggered by the violation of the momentum constraint, and both the Hamiltonian and the momentum constraints are affected by all the other constraints. Such an order of the constraint violation can be guessed in Fig. 11 (earlier time), where we plot the rate of constraint violation normalized with its initial value,  $||\delta\mathcal{C}||_2(t)/||\delta\mathcal{C}||_2(0)$ , as a function of time, for the gauge-wave testbeds with the plain BSSN evolution. (Note that the constraints at the initial time,  $\delta\mathcal{C}(0)$ , are not zero due to the numerical truncation error.) The parameters are the same as those shown in Sec. III A, and the lowest resolution run is used. From this investigation, we might conclude that to monitor the momentum constraint violation is the key to checking the stability of the evolution.

The second remark is on the Lagrange multipliers,  $\kappa$ , used in the adjusted systems. As discussed in Sec. IIB,

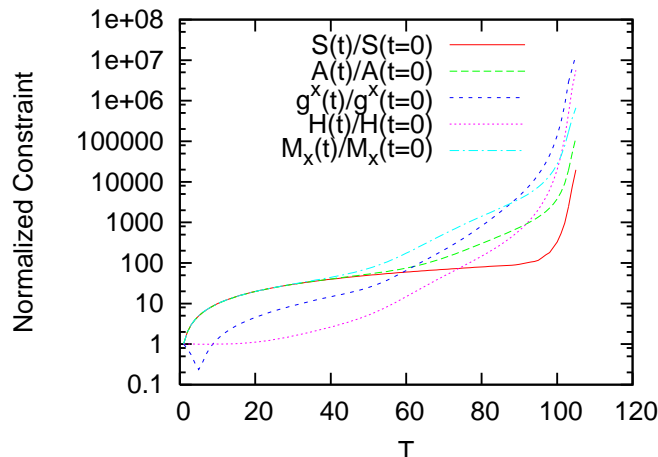


FIG. 11: The violation of all constraints normalized with their initial values,  $\|\delta\mathcal{C}\|_2(t)/\|\delta\mathcal{C}\|_2(0)$ , are plotted with a function of time. The evolutions of the gauge-wave testbeds with the plain BSSN system are shown. The parameters of the test are the same as those shown in Sec. III A, and the lowest resolution run,  $\rho = 2$ , is applied. By observing which constraint triggers the other constraint's violation from the constraint propagation equations, we may guess the mechanism by which the entire system is violating accuracy and stability. See the text for details.

the signatures of the  $\kappa$ s are determined *a priori*, and we confirmed that all the predicted signatures of  $\kappa$ s in [26] are right to produce positive effects for controlling constraint violations. However, we have to search for a suitable magnitude of  $\kappa$ s for each problem. Therefore we are now trying to develop a more sophisticated version, such as an auto-controlling  $\kappa$  system, which will be reported upon in the future elsewhere.

Although the testbeds used in this work are simple, it might be rather surprising to observe the expected effects of adjustments with such a slight change in the evolution equations. We therefore think that our demonstrations imply a potential to construct a robust system against constraint violations even in highly dynamical situations, such as black hole formation via gravitational collapse, or binary merger problems. We are now preparing our strong-field tests of the adjusted BSSN systems using large amplitude gravitational waves, black hole space-

time, or non-vacuum space-time, which will be reported on in the near future.

### Acknowledgments

K.K. thanks K. I. Maeda and S. Yamada for continuing encouragement. K.K. also thanks Y. Sekiguchi and M. Shibata for their useful comments on making numerical code. This work was supported in part by the Japan Society for Promotion of Science (JSPS) Research Fellowships and by a Grant-in-Aid for Scientific Programs. H.S. was partially supported by the Special Research Fund (Project No. 4244) of the Osaka Institute of Technology. A part of the numerical calculations was carried out on the Altix3700 BX2 at YITP at Kyoto University.

- 
- [1] M. Shibata, K. Taniguchi and K. Uryu, Phys. Rev. D **68**, 084020 (2003), Phys. Rev. D **71**, 084021 (2005)
- [2] M. Shibata and K. Taniguchi, Phys. Rev. D **73**, 064027 (2006)
- [3] P. Marronetti and S. L. Shapiro, Phys. Rev. D **68**, 104024 (2003)
- [4] P. Marronetti, M. D. Duez, S. L. Shapiro and T. W. Baumgarte, Phys. Rev. Lett. **92**, 141101 (2004)
- [5] J. A. Faber, T. W. Baumgarte, S. L. Shapiro and K. Taniguchi, Astrophys. J. **641**, L93 (2006)
- [6] F. Pretorius, Phys. Rev. Lett. **95**, 121101 (2005)
- [7] M. Campanelli, C. O. Lousto, P. Marronetti and Y. Zlochower, Phys. Rev. Lett. **96**, 111101 (2006)
- [8] J. G. Baker, J. Centrella, D-I. Choi, M. Koppitz, J. van Meter, Phys. Rev. Lett. **96**, 111102 (2006).
- [9] P. Diener, F. Herrmann, D. Pollney, E. Schnetter, E. Seidel, R. Takahashi, J. Thornburg, J. Ventrella, Phys. Rev. Lett. **96**, 121101 (2006)
- [10] F. Herrmann, I. Hinder, D. Shoemaker, P. Laguna, gr-qc/0601026v2
- [11] Z. B. Etienne, J. A. Faber, Y. T. Liu, S. L. Shapiro and T. W. Baumgarte, arXiv:0707.2083 [gr-qc].
- [12] W. Tichy and P. Marronetti, Phys. Rev. D **76**, 061502 (2007)
- [13] M. Campanelli, C. O. Lousto, Y. Zlochower and D. Merritt, Phys. Rev. Lett. **98**, 231102 (2007)
- [14] J. A. Gonzalez, M. D. Hannam, U. Sperhake, B. Bruggmann and S. Husa, Phys. Rev. Lett. **98**, 231101 (2007)

- [15] M. Campanelli, C. O. Lousto, Y. Zlochower and D. Merritt, *Astrophys. J.* **659**, L5 (2007)
- [16] J. Thornburg, P. Diener, D. Pollney, L. Rezzolla, E. Schnetter, E. Seidel and R. Takahashi, *Class. Quant. Grav.* **24**, 3911 (2007)
- [17] J. A. Gonzalez, U. Sperhake, B. Bruegmann, M. Hannam and S. Husa, *Phys. Rev. Lett.* **98**, 091101 (2007)
- [18] J. G. Baker, J. Centrella, D. I. Choi, M. Koppitz and J. van Meter, *Phys. Rev. D* **73**, 104002 (2006)
- [19] M. Shibata and K. Uryu, *Phys. Rev. D* **74**, 121503 (2006), *Class. Quant. Grav.* **24**, S125 (2007)
- [20] T.W. Baumgarte and S.L. Shapiro, *Phys. Rev. D* **59**, 024007 (1999).
- [21] T. Nakamura, K. Oohara and Y. Kojima, *Prog. Theor. Phys. Suppl.* **90**, 1 (1987). M. Shibata and T. Nakamura, *Phys. Rev. D* **52**, 5428 (1995).
- [22] T. Nakamura, K. Oohara and Y. Kojima, *Prog. Theor. Phys. Suppl.* **90**, 1 (1987). T. Nakamura and K. Oohara, in *Frontiers in Numerical Relativity* edited by C.R. Evans, L.S. Finn, and D.W. Hobill (Cambridge Univ. Press, Cambridge, England, 1989).
- [23] H. Beyer, and O. Sarbach, *Phys. Rev. D* **70**, 104004 (2004).
- [24] C. Gundlach, J. M. Martin-Garcia, *Phys. Rev. D* **74**, 024016 (2006).
- [25] H. Shinkai and G. Yoneda, gr-qc/0209111.
- [26] G. Yoneda and H. Shinkai, *Phys. Rev. D* **66**, 124003 (2002).
- [27] H. Shinkai and G. Yoneda, *Class. Quant. Grav.* **19**, 1027 (2002).
- [28] H-J. Yo, T.W. Baumgarte and S.L. Shapiro, *Phys. Rev. D* **66**, 084026 (2002).
- [29] M. Alcubierre *et al.*, *Class. Quant. Grav.* **21**, 589 (2004)
- [30] M. Boyle, L. Lindblom, H. P. Pfeiffer, M.A. Scheel, and L. E. Kidder, *Phys. Rev. D* **75**, 024006 (2007)
- [31] N. Jansen, B. Bruegmann and W. Tichy, *Phys. Rev. D* **74**, 084022 (2006)
- [32] Y. Zlochower, J. G. Baker, M. Campanelli and C. O. Lousto, *Phys. Rev. D* **72**, 024021 (2005)
- [33] B. Bruegmann, J. A. Gonzalez, M. Hannam, S. Husa, U. Sperhake and W. Tichy, arXiv:gr-qc/0610128.
- [34] M. Alcubierre, G. Allen B. Brüggmann, E. Seidel and W.-M. Suen *Phys. Rev. D* **62**, 124011 (2000)
- [35] M. Alcubierre *et al.*, *Phys. Rev. D* **62**, 044034 (2000)
- [36] H. -O. Kreiss and J. Olinger, *Methods for Approximate Solution of Time Dependent Problems* (GARP Publication Series, Geneva, 1973).
- [37] M. C. Babiuc *et al.* [Apples With Apples Collaboration], arXiv:0709.3559 [gr-qc].
- [38] M. Alcubierre, B. Bruegmann, P. Diener, M. Koppitz, D. Pollney, E. Seidel and R. Takahashi, *Phys. Rev. D* **67**, 084023 (2003)
- [39] S. A. Teukolsky, *Phys. Rev. D* **61**, 087501 (2000)
- [40] G. Yoneda and H. Shinkai, *Class. Quant. Grav.* **18**, 441 (2001).
- [41] M. Babiuc, B. Szilagyi and J. Winicour, in *Nalytical and Numerical Approaches to Mathematical Relativity* eds. by J. Frauendiener, D. Giulini, and V. Perlick, (Springer, Heidelberg, 2006). [arXiv:gr-qc/0404092].
- [42] W. Press, B. P. Flannery, S. Teukolosky, and W. T. Vetterling, *Numerical Recipes in C* (Cambridge University Press, Cambridge, England, 1986).